ICRH programmes for antennas and for
plasma dispersion relation

M. Söll, E. Springmann

IPP 4/215   Februar 1984

IPP

MAX-PLANCK-INSTITUT FÜR PLASMAPHYSIK

8046 GARCHING BEI MÜNCHEN

MAX-PLANCK-INSTITUT FÜR PLASMAPHYSIK

GARCHING BEI MÜNCHEN

ICRH programmes for antennas and for
plasma dispersion relation

M. Söll, E. Springmann

IPP 4/215   Februar 1984

Abstract

This report describes the computer programmes used for designing the
ICRH antennas at IPP.

In the first part of the report the underlying physical principles
are discussed on which the programmes are based. 2-D (two-dimensional)
and 3-D (three-dimensional) models are used.

In the second part the input and output of the programmes is described,
and in the third part some results on ICRH antennas built for existing
machines at IPP and antennas for machines which are in the design
and construction phase are presented.

In Appendix I the formulae for the 2-D model including plasma density
profiles are described and an investigation of this 2-D model on
folded dipol antennae is given.

In Appendix II the main formulae for a computer program for the
complete hot dispersion relation is given; the application of the
program for an ASDEX plasma (dispersion for the fast wave and
Bernstein wave) is shown.

Contents

I. Introduction

The ICRH antennas used in the last few years for coupling electro-magnetic power of up to 2 MW into plasmas have essentially all the same structure /9-11/ (stripline type antenna). They consist of two strips of conductors (central and return conductor) extending in the poloidal direction. They are fed at one end by a coax transmission line and short circuited at the other end. A schematic view of such an antenna is given in Fig. 1. In this figure an antenna is shown where the return conductor is placed between central conductor and vessel. In most cases the return conductor is integrated into the
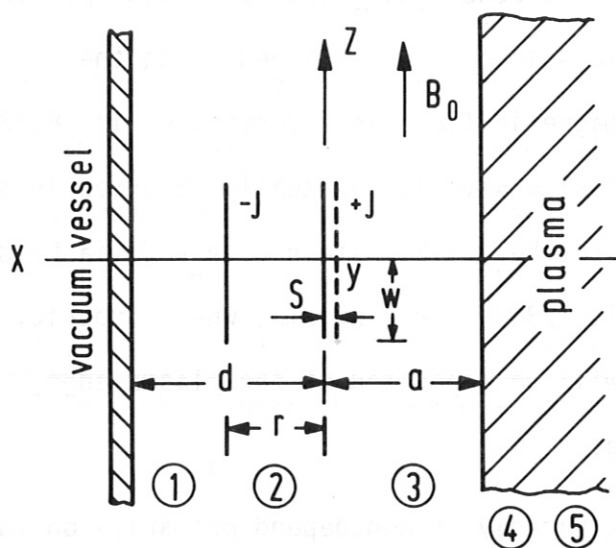
Fig. 1
Schematic representation of the antenna con-figuration with central conductor (at $x = 0$) and return conductor ($x = r$)

vessel (or liner /27/) yielding improved coupling properties with re-spect to the configuration of Fig. 1 /2, 4, 24/. The length of the central conductor is denoted by $2w_y$ (y: poloidal direction), and the width by $2w_z$ (z: direction into the toroidal direction). The distance between central conductor and return conductor is given by r and that to the vessel and plasma boundary respectively by d and a. The loop consisting of central- and return conductor is protected by two structures, the Faraday screen and lateral limiters. The Faraday screen

shown in Fig. 1 by a broken line is built generally by a slotted metal structure. The Faraday screen has a fourfold purpose: protecting the loop from charged particles and therefore to improve the electrical breakdown properties, to polarize the electromagnetic field produced by the currents flowing in the loop, to increase the capacitance of the antenna and therefore to increase the electrical length of it and finally to suppress waves which propagate between plasma and vessel. Electrical field components parallel to the total static magnetic field, composed from the toroidal field $\vec{B}_t$ and the poloidal field $\vec{B}_p$ have to be eliminated in order to minimize the production of the unwanted slow wave. The percentage of power going into the slow wave for antennas where the electrostatic shield is not aligned along the direction of the total static magnetic field is investigated in /8,13/. For a relative clean plasma the slow wave is eventually absorbed in the bulk plasma through conversion to the Ion-Bernstein wave and via Landau damping and ion cyclotron damping /34/. For a plasma, where impurity harmonics dominate, the power will be deposited at the plasma edge, yielding plasma surface heating.

The losses produced in the Faraday screen depend primarily on the conductivity of the material and on the blade width and gaps between the blades /12/. Experimental studies of power coupling through an electrostatic shield using resonant coupling loops show that coupling efficiencies in excess of 90 % were obtained /19, 37/.

In general antenna systems include two local limiters placed on either side of the antenna. They should protect the antenna from energetic particles. The limiters have to fullfil certain criterias otherwise they modify the antenna current distribution and the electromagnetic field. As studies show /14/, the presence of limiters can
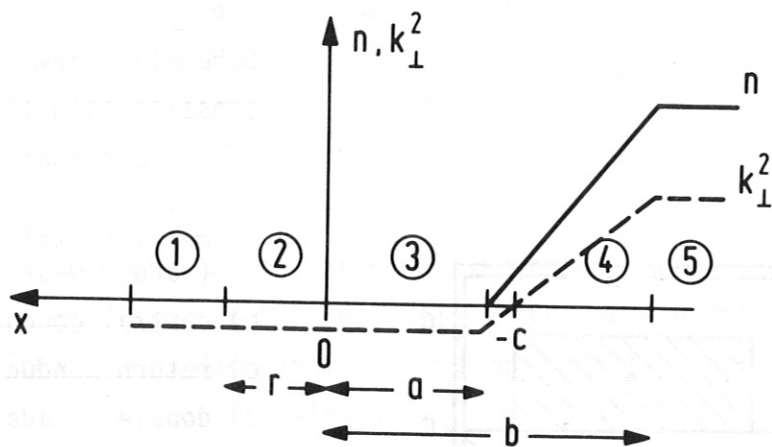
Fig. 2 Variation of the plasma density n and $k_\perp^2$. The distance between the vessel and plasma ($n=n_0$) is subdivided into four intervals with different E_y-fields.

reduce the coupling and therefore the efficiency of the antenna con-
siderably if unslotted limiters are used that are located closer to
the antenna than the distance central conductor return conductor.
In most present antenna designs the antennas are resonant; the length
of an antenna or an antenna unit is $\lambda/4$. Two antennas can be connected
back to back so that they share a common short circuit. In this case
the total length of this antenna is $\lambda/2$. Advantages of resonant antennas
are: reduced voltages in the coax transmission lines coupled directly
to the antenna and a reduction of the influence of the currents in the
feeders. A disadvantage, especially for antennas with rather high qua-
lity values is a strong variation of the antenna impedance by changes
in frequency or   antenna-plasma coupling. A method to increase the
electrical length of an antenna is to add internal capacitor elements
between the central- and return conductor (schematic view is given in
Fig. 3). Some possibilities are shown in Refs. /15, 22, 46/. The

Fig. 3

Schematic view of the cross-section (frontview) of the antenna:
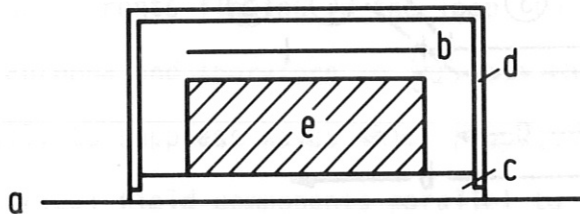
a) metallic wall (vacuum vessel)
b) central conductor
c) return conductor
d) double Faraday screen
e) additional capacitance

effectiveness of different internal capacitance systems have been investigated experimentally and compared with calculated antenna parameters /22/. As antenna impedance calculations show, the maximum input impedance values at the resonant frequency of an antenna with internal capacitance are smaller than the input impedance of the antenna without internal capacitance at the corresponding (higher) resonant frequency (comp. Figs. 7 and 12 of Ref. /7/).

Two-dimensional (2-D) /1, 2/ and three-dimensional (3-D) /5, 7, 8/ antenna theories have been developped in the last years. The important common features of the 2-D and 3-D theories are:

- single pass model (radiated power is completely absorbed in the plasma; no reflection of the incident wave).

- cold plasma dispersion relation.

- idealized Faraday screen (complete removal of the E_z field component; field in the toroidal direction, see Figs. 1, 2; anisotropic conductivity: $\sigma_{zz} = \infty$, $\sigma_{xx} = 0$).

The main differences between the 2-D and 3-D theories are:

- neglection of the current feeders in the 2-D model

- infinite antenna length in the 2-D model

- $k_y \equiv 0$ in the 2-D model

- the currents on the antenna elements are pregiven in the 2-D model (induced EMF-method); in two 3-D models developped by Theilhaber, Jacquinot /7/ and Puri /8/ the currents are calculated selfconsistently using a variational technique /35/.

One difference between the two selfconsistent theories should be mentioned; Puri takes into account the periodic antenna structure (in toroidal and poloidal direction) yielding a different antenna spectrum in comparison to a single loop antenna which is the model of Theilhaber and Jacquinot. The spectrum of a periodic antenna is not concentrated at $n_y = n_z = 0$ as in the case of a single loop antenna, where n_z and n_y are the components of the refractive index $\vec{n}$ in the y and z direction.

II. Calculation models

In the following we describe models on which the antenna calculation programmes are based.

1. The 2-D model

The calculation model is based on principles described in /1, 2/. Only the E_y-field component producing the magnetosonic wave in the plasma is taken into account.

The central conductor (see Fig. 1) is placed at $x = 0$. The distance to the first wall is d, and to the return conductor is r. The current density $\vec{j}_o$ in the central conductor is directed into the positive

y-direction, and that of the return conductor into the opposite direction. The plasma boundary is a distance a apart from the central conductor. The plasma density increases from $x = -a$ to the maximum value at $x = -b$ (see Fig. 2).

The distance between the vessel and the position where the plasma reaches maximum density ($n = n_o$) is divided into four intervals (see Fig. 2).

In the intervals (1), (2) and (3) the fields are obtained by the solution of the vacuum field equation which is given by

$$(\frac{d^2}{dx^2} - p^2)\omega B_z = 0 \tag{1}$$

$$\omega B_{zm} = A_m e^{-px} + B_m e^{px} \tag{2}$$

The electric field component E_{ym} follows from

$$E_{ym} = \frac{i}{p^2} \frac{d}{dx} \omega B_{zm} \tag{3}$$

where A_m and B_m are arbitrary constants to be determined in region m and $p^2 = k_{\shortparallel}^2 - k_o^2$. k_o is the vacuum propagation constant $k_o = \omega/c$ and $k_{\shortparallel}$ is given by $k_{\shortparallel} = n/R_o$ where R_o is the major torus radius.

In the plasma regions (4) and (5) the magnetosonic waves are described by the following sets of equations /2/

$$(\frac{d^2}{dx^2} + k_{\perp}^2) B_x = 0 \tag{4}$$

$$E_y = - \frac{\omega B_x}{k_{\shortparallel}} \tag{5}$$

$$\omega B_z = \frac{i}{k_{\shortparallel}} \frac{d}{dx} \omega B_x \tag{6}$$

The perpendicular wave vector $k_\perp$ follows from the dispersion relation

$$k_\perp^2 = k_0^2 \, \varepsilon_1 - k_\parallel^2 - k_0^4 \, \varepsilon_2^2/(k_0^2\varepsilon_1 - k_\parallel^2) \tag{7}$$

where ε_1 and ε_2 are the cold plasma dielectric tensor elements.

$$\overline{\varepsilon} = \begin{bmatrix} \varepsilon_1 & i\varepsilon_2 & 0 \\ i\varepsilon_2 & \varepsilon_1 & 0 \\ 0 & 0 & \varepsilon_3 \end{bmatrix} \tag{8}$$

$$\varepsilon_1 = 1 - \sum_s \omega_{ps}^2/(\omega^2 - \omega_{cs}^2) \tag{9}$$

$$\varepsilon_2 = \sum_s E_s \, \omega_{cs} \, \omega_{ps}^2/[\omega(\omega^2 - \omega_{cs}^2)] \tag{10}$$

$$\varepsilon_3 = 1 - \sum_s \omega_{ps}^2/\omega^2 \tag{11}$$

E_s is the sign of charge, ω_{cs} is the cyclotron frequency and ω_{ps} the plasma frequency of the particle of species s.

For $\omega = 0$ (ω_{ci}) and for one particle species s the relation (7) (and $B = B_0 = \text{const}$) reduces to

$$k_\perp^2 = \frac{[\omega^2/V_A^2 - k_\parallel^2 \, (1 - \omega/\omega_c)] \, [\omega^2/V_A^2 - k_\parallel^2 \, (1 + \omega/\omega_c)]}{\omega^2/V_A^2 - k_\parallel^2 \, (1 - \omega^2/\omega_c^2)} \tag{12}$$

where V_A is the Alfvén velocity $V_A = \omega_{ci}^2/\omega_{pi}^2 \, \mu_0 \varepsilon_0$.

As shown in Appendix II, the approximation of the plasma by a cold dielectric tensor is well justified as far as the coupling of the fast wave is considered.

From (12) it follows that $k_\perp^2 = -k_\parallel^2$ for $n = 0$ (vacuum) and $k_\perp = 0$ for $\omega^2/V_A^2 = k_{\parallel \, max}^2 \, (1 + \omega/\omega_c)$.

In region ④ a linear profile for $k_\perp^2$ is assumed (which approximates well the density profiles of the plasma machines investigated). The model is described in detail in Ref. /36/.

The solution of the differential equation (4) is given by a linear superposition of Airy functions of argument $2/3\ A\xi^{3/2}$ with

$$A^2 = k_\parallel^2/(c-a) \qquad c = \frac{a + b\ k_\parallel^2/k_{\perp b}^2}{1 + k_\parallel^2/k_{\perp b}^2} \qquad \xi = -(c+x) \qquad (13)$$

$x = -c$ is the cut-off position for $k_\perp^2$ and $k_{\perp b}$ is the $k_\perp$ value at maximum density $(x = -b,\ n = n_0)$.

The solution has the form

$$\omega B_{x3} = A_4\ \xi^{1/2}\ J_{1/3}\ (2/3\ A\xi^{3/2}) + B_4\ \xi^{1/2}\ J_{-1/3}\ (2/3\ A\ \xi^{3/2}) \quad (14)$$

where $J_{\pm 1/3}$ are Bessel functions. With the equations 5 and 6 E_{y3} and B_{z3} follow from ωB_{x3}.

According to the single pass absorption, no reflected wave is present in region ⑤ $(\infty - x < -b)$ and therefore only the solution propagating towards $x = -\infty$ is retained. Thus the fields in region 5 are given by

$$\omega B_z = A_5 e^{-ik_{\perp b}x}$$

To determine the arbitrary constants $A_1 \dots A_5$ the usual boundary conditions (see /1, 2/) are applied.

$x = d$ $E_{y1} = 0$

$x = r$ $E_{y1} = E_{y2}$

$$\omega B_{z2} - \omega B_{z1} = \mu_o \, \omega J_r(k_{\shortparallel})$$

$x = 0$ $E_{y2} = E_{y3}$

$$\omega B_{z3} - \omega B_{z2} = \mu_o \, \omega J_o(k_{\shortparallel}) \tag{16}$$

$x = -a$ $E_{y3} = E_{y4}$

$$\omega B_{z3} - \omega B_{z4} = 0$$

$x = -d$ $E_{y4} = E_{y5}$

$$\omega B_{z4} - \omega B_{z5} = 0$$

$J_o(k_{\shortparallel})$ and $J_r(k_{\shortparallel})$ are the Fourier Transform of the current densities in the central conductor and return conductor. For a constant current density across the width of the conductor the current density is given for a total current I by

$$J(k_{\shortparallel}) = I \, \frac{\sin(k_{\shortparallel} w_z)}{k_{\shortparallel} w_z} \tag{17}$$

and for current density profile peaked at the boundaries $(z = \pm w_z)$ /36/

$$J(k_{\shortparallel}) = \lambda \, [\pi w_z \beta \, J_o(k_{\shortparallel} w_z) + 2\alpha w_z \, \frac{\sin(k_{\shortparallel} w_z)}{k_{\shortparallel} w_z}] \tag{18}$$

where

$$\beta = (4d/\pi w_z)^{1/2}, \; \alpha = 1 + d/w_z \pi - \beta, \; \lambda = I/(2w_z \alpha + \pi w_z \beta) \tag{19}$$

The specific resistance R_2 and inductance L_2 (the subscript 2 refers the two-dimensionality of the model) follows from the procedure described in /5/. The complex power radiated by the antenna is given by

$$P = -1/2 \iiint \vec{E} \cdot \vec{J}^* \, dV$$

$$= -1/2 \iint [J_o^*(z) \, E_y(z)|_{x=0} + J_r^*(z) \, E_y(z)|_{x=r}] \, dydz \qquad (20)$$

For the 2-D model $\partial/\partial_y \equiv 0$, the integration over dy gives the length of the antenna $2w_y$. Relation (20) can be rewritten for the power per unit length p

$$P/2w_y = p = -1/2 \int [J_o^* \, E_y|_{x=0} + J_r^* \, E_y|_{x=r}] \, dz \qquad (20')$$

Using Parseval's theorem /48/, the expression (20) can be computed from the Fourier spectra of currents and fields

$$p = -\frac{1}{4\pi} \int [J_o^*(k_{"}) \cdot E_y(k_{"})|_{x=0} + J_r^*(k_{"}) \, E_y(k_{"})|_{x=r}] \, dk_{"} \qquad (21)$$

The power of the antenna can be written in terms of the input impedance Z_A and the input current I_A as

$$P = \frac{1}{2} Z_A |I_A|^2 \qquad (22)$$

Z_A is the input impedance and I_A is the input current.

In transmission line theory the power is related to R_2 and L_2 by /44/

$$\frac{1}{2} Z_A |I_A|^2 = \frac{1}{2} \int_0^{2w_y} R_2 |I|^2 \, dy - \frac{i\omega}{2} \int_0^{2w_y} L_2 |I|^2 \, dy \qquad (23)$$

Comparing (21) and (23) the specific resistance R_2 and the specific inductance L_2 can be computed from

$$(R_2 - i\omega L_2) |I|^2 = 2 p \qquad (24)$$

$$|I|^2 (R_2 - i\omega L_2) = -\frac{1}{2\pi} \int [J_o^*(k_{"}) E_y(k_{"})|_{x=0} + J_r^*(k_{"}) E_y(k_{"})|_{x=r}] \, dk_{"} \qquad (25)$$

The current density in the return conductor can be related to the current density in the central conductor by

$$J_r(k_{\shortparallel}) = \text{sign} \; J_o \cdot F \; (w_{zo}, w_{zr}) \qquad (26)$$

where the absolute value of total current flowing in the return I_r and central conductor I_o is equal

$$|I| = \int\limits_{-w_{zr}}^{+w_{zr}} |J_r| dz = \int\limits_{-w_{zo}}^{+w_{zo}} |J_o| dz \qquad (27)$$

and sign = + for $\vec{I}_o \uparrow\uparrow \vec{I}_r$ and sign = - for $\vec{I}_o \downarrow\uparrow \vec{I}_r$.

Relation (26) takes into account that in antenna designs the width of the two conductors can be different ($2w_{zo} \neq 2w_{zr}$).

Introducing geometrical functions g_2' and h_2' as in Ref. /2/, which are functions depending only on geometric parameters, the relation (25) can be rewritten as

$$|I|^2 \; (R_2 - i\omega L_2) = -\frac{\mu_o \omega}{4\pi^2} \int [g' - ih'] \; |J_o|^2 \; dk_{\shortparallel} \qquad (28)$$

Finally the specific resistivity and inductance are obtained

$$R_2 = -\frac{\mu_o \omega}{2\pi |I|^2} \int\limits_{-\infty}^{+\infty} g'(k_{\shortparallel}) \; |J_o|^2 \; dk_{\shortparallel} \qquad (29)$$

$$L_2 = \frac{-\mu_o}{2\pi |I|^2} \int h'(k_{\shortparallel}) \; |J_o|^2 \; d_{k_{\shortparallel}} \qquad (30)$$

In the following, expressions for the electric field E_y and for g' and h' are derived for the special case that a = b (step function for the density profile). The more complex formula where a plasma density is taken into account and which are used in the computer program are de-scribed in the Appendix I.

The electrical field component E_y at $x = 0$ and $x = r$ follow from the procedure described before as:

$$E_y|_{x=0} = \frac{i}{p} \mu_0 \omega \frac{2 J_r K + J_0 [e^{-pr}(K-1) + e^{pr}(K-1)]}{e^{pr}(1+K)(B+1) + (K-1) e^{-pr}(B-1)} \tag{31}$$

$$E_y|_{x=r} = \frac{i}{p} \mu_0 \omega K \frac{\{J_r [(B+1)e^{pr} - e^{-pr}(B-1)] + 2 J_0\}}{e^{pr}(1+K)(B+1) + (B-1)(K-1) e^{-pr}} \tag{32}$$

$$K = \frac{1 - e^{-2p(d-r)}}{1 + e^{-2p(d-r)}} \tag{33}$$

$$B = \frac{p(e^{-2pb} - 1) + i k_{\perp b}(1 + e^{-2pb})}{-p(1 + e^{-2pb}) + i k_{\perp b}(1 - e^{-2pb})} \tag{34}$$

As can be seen from (33), K as a function only of the distance between return conductor and vessel, tends to zero as the return conductor approaches the vessel, ($K = 0$, $r = d$). Therefore $E_y|_{x=r \to d} \to 0$ (see boundary condition 16) and $E_y|_{x=0}$ depends then only on J_0, the current density on the central conductor.

From (31) and (32) follows that the electric field E_y can be influenced also by the value of J_r, which can be varied by using different widths of the return conductor.

For the special case $J_r = -J_0$ (and $|I_r| = |I_0| = I$) and $r \neq d$ the functions g' and h' are:

$$g' = - \frac{e^{-2pb}(1-e^{-2pd} - C)^2 k_{\perp b}}{p^2(1 + e^{-2p(d+b)})^2 + k^2_{\perp b}(1 - e^{-2p(d+b)})^2} \tag{35}$$

$$-h' = h'_o + h'_p \tag{36}$$

$$h'_o = \frac{1 - e^{-2pd} - C(2 - e^{pr})}{2p} \tag{37}$$

$$h'_p = \begin{cases} \dfrac{e^{-2pb}}{2p} \dfrac{[(1-e^{-2pd})^2 + C[C-2-2e^{-2pd}]\,[p^2(1+e^{-2p(d+b)}] - k^2_{\perp b}(1-e^{-2p(d+b)})]}{p^2(1+e^{-2p(d+b)})^2 + k^2_{\perp b}(1-e^{-2p(d+b)})^2} \\ \qquad\qquad\qquad\qquad\qquad\qquad\qquad\qquad\qquad\qquad \text{for } k_{\parallel} < k_{\parallel\,max} \\[4pt] \dfrac{e^{-2pb}}{2p} \cdot \dfrac{[(1-e^{-2pd})^2 + C[C-2+2e^{-2pd}]\,[p-|k_{\perp b}|]}{p(1+e^{-2p(d+b)}) + |k_{\perp b}|\,(1-e^{-2p(d+b)})} \tag{39} \end{cases}$$

$$\text{for } k_{\parallel} > k_{\parallel\,max}$$

$$\text{where } k_{\perp b}(k_{\parallel\,max}) = 0$$

$$p = +\sqrt{k^2_{\parallel}} \;,\quad C = e^{+pr}(e^{-2pr} - e^{-2pd}) \tag{40}$$

The term h'_o gives the specific inductance L_2 in the absence of the plasma, and the term h'_p involves the influence of the plasma.

The influence of the return conductor on the antenna function g' and h' (and therefore on R_2 and L_2) is given by the term C, which reduces g' and R_2 (see for an example Ref. /24/).

When the return conductor is integrated into the vessel, the formulas derived in Refs. /2, 3, 6/ are obtained (C = 0 for r = d and a = b):

$$g' = -\frac{e^{-2pb}(1-e^{-2pd})^2\, k_{\perp b}}{p^2(1+e^{-2p(d+b)})^2 + k^2_{\perp b}(1-e^{-2p(d+b)})^2} \tag{35'}$$

$$h'_o = \frac{1 - e^{-2pd}}{2p} \tag{37'}$$

$$h'_p = \frac{e^{-2pb}}{2p}\,\frac{(1-e^{-2pd})^2}{}\,\frac{p^2(1+e^{-2p(d+b)}) - k^2_{\perp b}(1-e^{-2p(d+b)})}{p^2(1+e^{-2p(d+b)})^2 + k^2_{\perp b}(1-e^{-2p(d+b)})^2} \tag{38'}$$

$$h'_p = \frac{e^{-2pb}}{2p} (1-e^{-2pd})^2 \frac{p - |k_{\perp b}|}{p(1+e^{-2p(d+b)}) + |k_{\perp b}|(1-e^{-2p(d+b)})} \qquad (39')$$

In the 2-D model the specific capacitance C_2 is computed separately using the formula of Ref. /2/ (electrostatic calculation)

$$\frac{1}{C_2} = - \frac{1}{\pi\varepsilon_0} \sum_{m=1}^{\infty} \frac{(1-e^{2|k_{||}|s})(1-e^{-2|k_{||}|d})}{e^{2|k_{||}|s} - e^{-2|k_{||}|d}} \frac{1}{m} (\sin \frac{\pi m}{2})^2 (\frac{\sin k_{||} w_z}{k_{||} w_z})^2 \qquad (41)$$

where $k_{||} = \frac{m \cdot}{2 P_z}$ ($2 P_z$ = total width in toroidal direction of the Faraday screen), s = radial distance between central conductor and Faraday screen (see Fig. 4). Formula (41) is used for the cases where
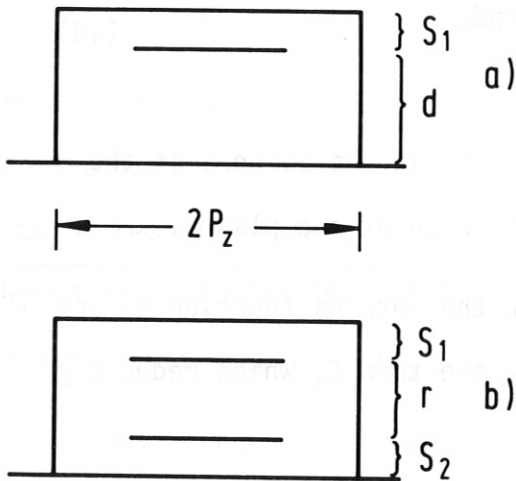

Fig. 4

Schematic view of the cross-section of an ICRH antenna with

a) return conductor integrated into the vessel

b) return conductor in front of the vessel

where the return conductor is integrated into the vessel. For antennas with an internal capacitance structure between central conductor and return conductor the distance d (only in rel. (41)) is decreased to d' = d - dc (where dc is the hight of the internal capacitance structure).

Formula (41) was derived in Ref. /2/ by calculating the TM mode confined within the screen.

In comparison to formula (41) we present the formulas following for a single transmission line. For a transmission line the specific capacitance is given by

$$C = \varepsilon_0 \cdot \frac{2 w_z}{d} \tag{42}$$

For an antenna with a Faraday screen (see Fig. 4) and the return conductor integrated into the vessel this would result in

$$C = \varepsilon_0 \cdot 2 w_z \frac{s_1 + d}{s_1 \cdot d} \tag{43}$$

For antennas with the return conductor (see Fig. 5) placed between vessel and central conductor the specific capacitance is given by $(w_{zr} = w_{zo})$

$$C_{\uparrow\downarrow} = \varepsilon_0 \cdot 2 w_{zo} \frac{2s_1 s_2 + r(s_1 + s_2)}{s_1 \cdot s_2 \cdot r} \tag{44}$$

when $\vec{J}_o = -\vec{J}_r$ (antiparallel) and

$$C_{\uparrow\uparrow} \cong \varepsilon_0 \cdot 2 w_{zo} \frac{s_1 + s_2}{s_1 \cdot s_2} \tag{45}$$

for $\vec{J}_o = \vec{J}_r$ (parallel).

For the specific capacitance $C_{\uparrow\downarrow}$ the two capacitances C_1 and C_2 of the central conductor and return conductor are added $(C_1 + C_2)$ and for the $C_{\uparrow\uparrow}$ the capacitance between the central and return conductor is neglected.

A comparison of C calculated from formulæ (41) and (42) with data from an ASDEX like antenna ($s_1 = 1.4$ cm; d = 6.9 cm; 2 P_z = 26 cm) are collected in Table I.
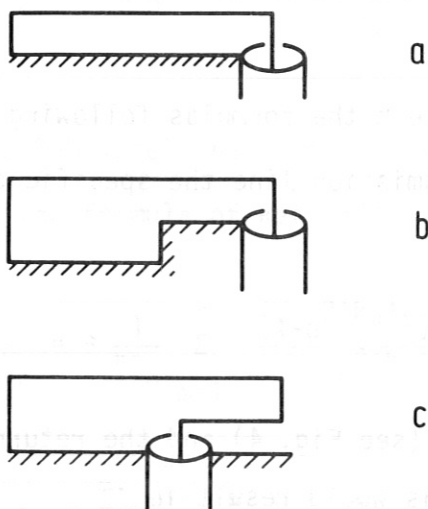
Fig. 5

Possible antenna configuration for ASDEX Upgrade

	Formula (41)	Formula (42)	Specification
C F/m	$1.37 \cdot 10^{-10}$	$1.5 \cdot 10^{-10}$	$s_1 = 1.4$ cm without internal capacitance
C F/m	$2.73 \cdot 10^{-10}$	$2.80 \cdot 10^{-10}$	$s_1 = 1.4$ cm with int.capacitance

Table I: Comparison of the specific capacitance calculated from formulae (41) and (43) for an ASDEX antenna with and without additional (internal) capacitance

The input impedance of the antenna and the maximum voltage at the antenna input can be calculated using transmission line theory. In terms of R_2, L_2 and C_2, for which the formulas are given above, the input impedance Z_A of an antenna short circuited at the end is given by

$$Z_A = Z_o \tanh(\gamma \ell) \tag{46}$$

$$Z_o \cong \left\{ \frac{R_2 + i\omega L_2}{i\omega C_2} \right\}^{1/2} \qquad \gamma = \left\{ (R_2 + i\omega L_2) i\omega C_2 \right\}^{1/2} \tag{47}$$

and the maximum voltage on the antenna V_M and the input voltage V_A

$$V_M = 2 Z_o' \left\{ \frac{P}{R_2 \ell \ (1 + \sin 2\beta \ell / (2\beta \ell)} \right\}^{1/2} \qquad \beta \ell > \pi/2 \tag{48}$$

$$V_A = 2 Z_o' \left\{ \frac{P}{R_2 \ell (1 + \sin 2\beta \ell / 2\beta \ell)} \right\}^{1/2} \sin \beta \ell \qquad \beta \ell < \pi/2 \tag{49}$$

$\ell \equiv 2 w_y$ is the length of the central conductor, P is the active power and $Z_o' = \sqrt{L_2/C_2} - i R_2/2\beta$, $\beta = \omega \sqrt{L_2 C_2}$.

From the input impedance the maximum voltage occuring on the (coax) line can be calculated.

Since the active or net power P flowing through a coax line with a characteristic impedance Z_c to the antenna is related to the maximum voltage on the line by /38/

$$P = \frac{1}{2} \frac{1}{Z_c} \frac{1 - |R|}{1 + |R|} \cdot |V_{max}|^2 \tag{50}$$

where $\qquad |R| = \left| \frac{Z_A - Z_c}{Z_A + Z_c} \right| \tag{51}$

we obtain $|V_{max}| = \left\{ 2 P Z_c \frac{1 + |R|}{1 - |R|} \right\}^{1/2}$.

2. Extended 2D-Models

In the standard 2-D models the distance central conductor - return conductor was assumed constant; in the following these antennas will be named as "normal antennas". It is possible to extend these 2-D models to different shapes, these are shown schematically in Fig. 5. The step antenna (Fig. 5b) is characterized by a discontinuity in the distance between central conductor and return conductor. The so-called "trombone" antenna (Fig. 5c) is used for the JET ICRH experiments /4/.

Step antenna

The step antenna is treated as a transmission line with two different sections as shown in Fig. 6.
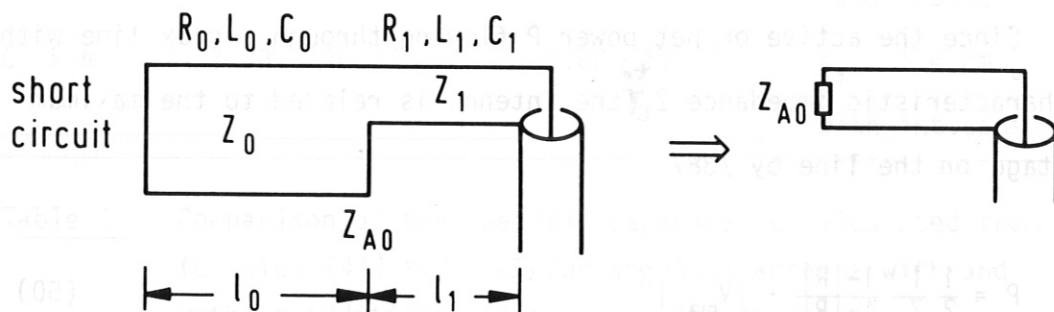

Fig. 6 Step antenna and the equivalent circuit

With the 2-D model R_o, L_o, C_o, R_1, L_1, C_1 is calculated, then the impedance Z_{AO}

$$Z_{AO} = Z_o \tanh(\gamma_o \ell_o) \qquad (52)$$

and finally Z_{A1}

$$Z_{A1} = \frac{Z_{A0}\cosh(\gamma_1\ell_1) + Z_1\sinh(\gamma_1\ell_1)}{\cosh(\gamma_1\ell_1) + (Z_{A0}/Z_1)\sinh(\gamma_1\ell_1)} \tag{53}$$

where γ_0, γ_1, Z_0, Z_1 are given by the formulas (47).

Trombone Antenna

The exact treatment of a trombone antenna based on transmission line theory is given in Ref. /4/. The trombone antenna is there subdivided into two parts as shown in Fig. 7 (page 13, Ref. 4).
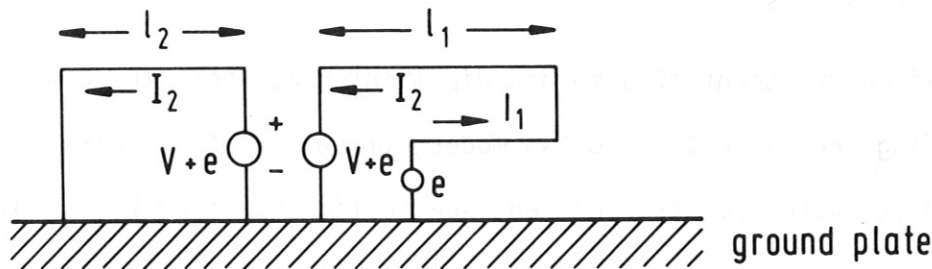

Fig. 7   Subdivision of the trombone antenna into two parts.

The currents I_1 and I_2 must be assumed unequal, as the right hand side of the antenna is unbalanced. The left part of the antenna can be treated as a short-circuited transmission line with an input impedance Z_2 (formulae (46), 47)).

The right hand side is further subdivided in a symmetric and an antisymmetric transmission line with symmetric and antisymmetric currents (where the assumption is made, that the potentials of the two conductors are equal). The input impedance Z_S of the symmetric transmission line, which is taken as an open ended one, follows from

$$Z_S = Z_{0s}\,\mathrm{cth}\,(\gamma_s\ell_1). \tag{54}$$

The R-, L- and C-values for the symmetric transmission line are calculated with the 2-D model, where $\vec{J}_r = \vec{J}_o$ (see eqs. (20), (21) and (45)).

The R-, L- and C-values for the antisymmetric transmission line are calculated likewise with the 2-D model where $\vec{J}_r = -\vec{J}_o$ (see eqs. (20), (21) and (44)), and the input impedance Z_a by the formula for a short-circuited transmission line (see eqs. (46), (47)).

The total input impedance Z can be calculated from Z_2, Z_s, Z_a by /4/

$$Z = \frac{4\, Z_s Z_2 + Z_a Z_2 + 4\, Z_a Z_s}{4\, Z_2 + Z_a + 4\, Z_s} \tag{55}$$

(For a detailed treatment of a folded dipole antenna, where the concept of subdividing the currents into two modes, one with antisymmetric current and one with symmetric current see Section 5.2 from Ref. /43/).

3. 3-D Models

In the 2-D model the antenna is infinitely long, the feeders are not taken into account and there is no Fourier decomposition with respect to k_y ($k_y \equiv 0$, $dI/dy \equiv 0$). The influence on these simplification on the antenna parameters seems large. Thus 3-D antenna calculation programs had to be installed or developped at our institute; one of them (so-called 3-D_{QS}, quasi static limit*) is based on the theory developed at Brussels /5/, where the underlying principle is the induced emf-method.

_____

* quasi static limit: $\beta = 0$ and k_o is neglected with respect to $k_{\parallel}$ and k_y in the vacuum field equation. (ASDEX parameter: $k_{\parallel min} = 0.66$; $k_{y\ min} = 2.5$ and $k_o = 1.4$)

A copy of the 3-D antenna program, BARBAR /7/, where the currents and fields are self-consistently determined, which was developped at Fontenay-aux-Roses /7/, was also implemented here. A similar self-consistent 3-D antenna program was developped at our institute /8, 17/; it is extensively described in /8, 17/ and will not be discussed in this report.

The 3-D$_{QS}$ program

Similar as in the 2-D model the antenna input impedance Z_A can be written as the energy conservation equation of a transmission line /44/

$$\frac{1}{2} Z_A |I_A|^2 = \frac{1}{2} R_3 \int_0^{2w_y} |I|^2 \, dy - \frac{i\omega L_3}{2} \int_0^{2w_y} |I|^2 \, dy - \frac{1}{2i\omega C_3} \int_0^{2w_y} |dI/dy|^2 dy \tag{56}$$

From (56), R_3, L_3 and C_3 follow.

The 3-D$_{QS}$ computer program was developed for the simplified model that $J_y(y,z)$ is constant over the antenna in y and z direction. As a result the last term in (56) is equal to zero. Further an infinitely steep density gradient of the plasma at the plasma edge at x = -a = -b is assumed (constant plasma density over the plasma radius). Similar as for the 2-D case the Fourier components of the electrical field E_y can be written as: $E_y \sim g_3 - ih_3$, where /5/

$$g_3' - ih_3' = \frac{-ip}{k_0^2 - k_\parallel''} \left\{ \frac{[\xi \cosh(pa) - \sinh(pa)] \sinh(pd)}{\xi \cosh[p(a+d)] - \sinh[p(a+d)]} \right\} \tag{57}$$

$$\xi = \frac{k_\parallel'' - k_0^2}{p \, k_{\perp b}^2} [\mu k_y - i \sqrt{k_{\perp b} - k_y^2}] \tag{58}$$
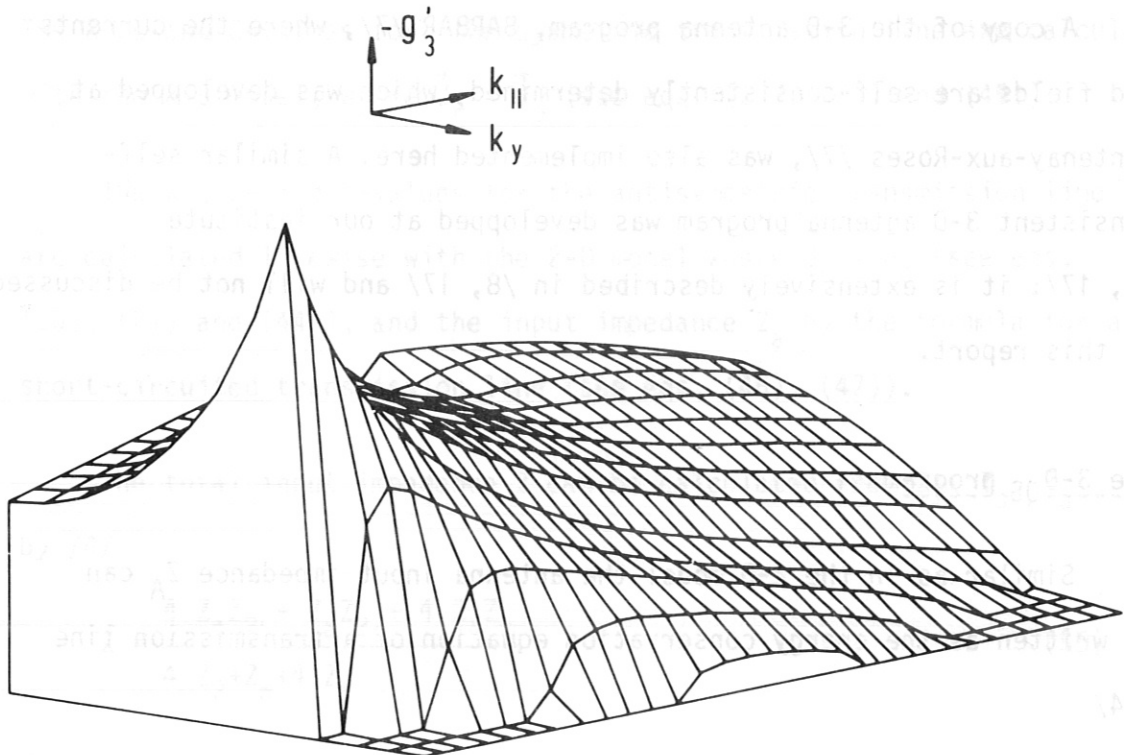
Fig. 8 Three-dimensional plot of the function g_3' versus $k_\parallel$ and k_y.
$a=b=7\text{cm}$; $d=7\text{cm}$; $n_o=5\cdot10^{13}\text{cm}^{-3}$; $f=70$ MHz; $w_z=11$ cm; $w_y=44\text{cm}$.

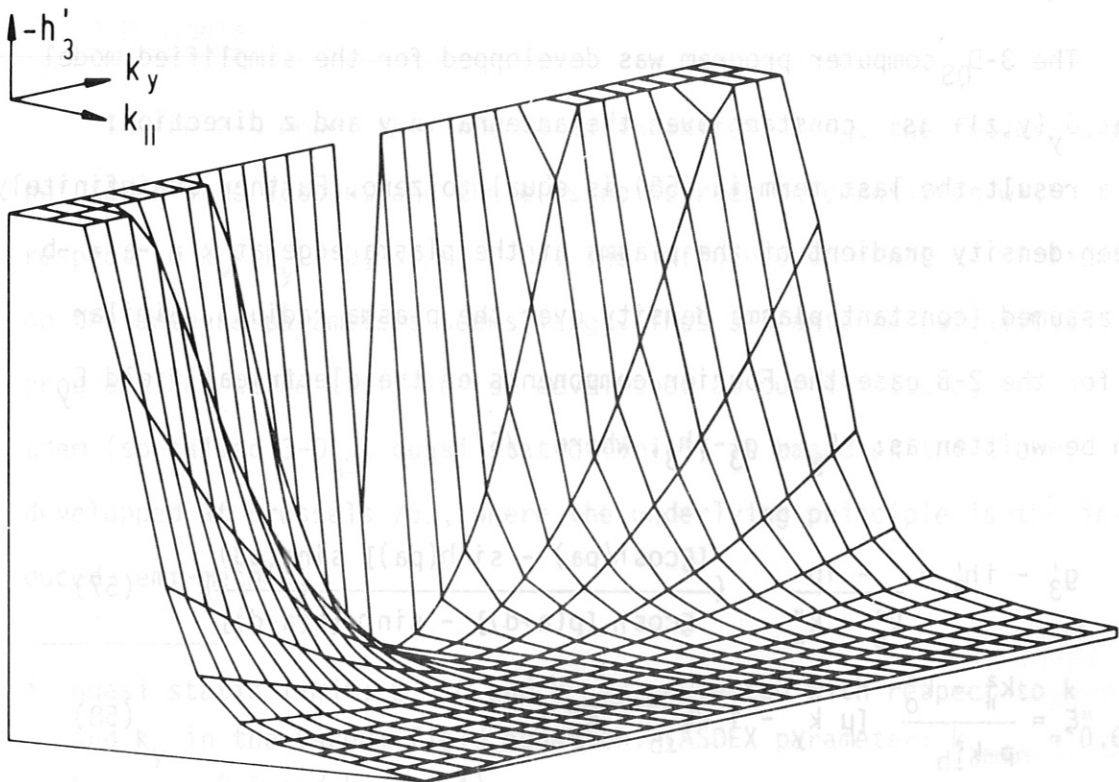**Fig. 9** Three-dimensional plot of h_3' versus $k_\parallel$ and k_y.

$$p = [k_y^2 + k_{\shortparallel}^2 - k_o^2]^{1/2} \tag{59}$$

$$\mu = k_o^2 \, \varepsilon_2 / [k_o^2 \, \varepsilon_1 - k_{\shortparallel}^2] \tag{60}$$

$$k_{\perp b}^2 = k_o^2 \, \varepsilon_1 - k_{\shortparallel}^2 - k_o^2 \, \varepsilon_2 \, \mu \tag{61}$$

ε_1 and ε_2 are the cold plasma dielectric tensor elements (see relations (9) and (10)).

A plot of $-g_3'$ and $-h_3'$ as a function of k_y and $k_{\shortparallel}$ is shown in Figs. 8 and 9. g_3' is asymmetric with respect to k_y and exhibits a maximum at positive values of this variable. (For a further discussion see Ref. /4/). (The transition of g_3-ih_3 to g_2-ih_2 is given by setting $k_o = 0$ and $k_y = 0$).

The specific resistivity R_3 and specific inductance L_3 per unit length are calculated from

$$R_3 = - \frac{\mu_o \omega}{2\pi} \int_{-\infty}^{\infty} G'(k_{\shortparallel}) |J_1|^2 \, dk_{\shortparallel} \tag{62}$$

with

$$G'(k_{\shortparallel}) = \frac{1}{\pi w_y} \int_{-\infty}^{\infty} g_3' \, \frac{k_{\shortparallel}^4}{p^4} \, |J_2|^2 \, dk_y \tag{63}$$

and

$$|J_1|^2 = \left| \frac{\sin k_{\shortparallel} w_z}{k_{\shortparallel} w_z} \right|^2$$

$$|J_2|^2 = \left| \frac{\sin k_y w_y}{k_y} \right|^2 \tag{64}$$

$$L_3 = - \frac{\mu_o}{2\pi} \int_{-\infty}^{\infty} H'(k_{\shortparallel}) \, |J_1|^2 \, dk_{\shortparallel} \tag{65}$$

with

$$H'(k_{\shortparallel}) = \frac{1}{\pi w_y} \int_{-\infty}^{\infty} [h_3' \, \frac{k_{\shortparallel}^4}{p^4} + d \, \frac{k_y^2}{p^2}] \, |J_2|^2 \, dk_y \tag{66}$$

The functions $|J_1|^2$ and $|J_2|^2$ are given by the Fourier transformed current density $J_y(y,z)$ which is assumed to be constant across the conductor width $2\,w_z$ and along the conductor length $2\,w_y$ and is given by

$$J_y(k_{\shortparallel},\, k_y) = 2\, I_o\, \frac{\sin k_{\shortparallel}\, w_z}{k_{\shortparallel}\, w_z} \cdot \frac{\sin k_y\, w_y}{k_y}\, e^{-ik_y\, w_y} \tag{67}$$

The factors $k_{\shortparallel}^4/p^4$ and an additional imaginary part $d\,\dfrac{k_y^2}{p^2}$ (d is the distance between central conductor and return conductor) come from the fact that the feeders were taken into account. $k_{\shortparallel}^4/p^4$ is always smaller than or equal to one and therefore R_3 is reduced with respect to R_2 by the inclusion of the feeders, as is demonstrated in Fig. 10, where R_3' and R_2' and $\omega L_3'$ and $\omega L_2'$ are compared for an ASDEX antenna.

$$R_3' = -\frac{\mu_o \omega}{2\pi}\, G'\, |J_1|^2$$

$$R_2' = -\frac{\mu_o \omega}{2\pi}\, g'\, |J_1|^2$$

$$\tag{68}$$

$$\omega L_3' = -\frac{\mu_o \omega}{2\pi}\, H'\, |J_1|^2$$

$$\omega L_2' = -\frac{\mu_o \omega}{2\pi}\, h'\, |J_1|^2$$

Integrating R' and L' with respect to $k_{\shortparallel}$ yields the following values

$$R_2 = 7.8\ \Omega/m$$

$$R_3 = 3.5\ \Omega/m$$

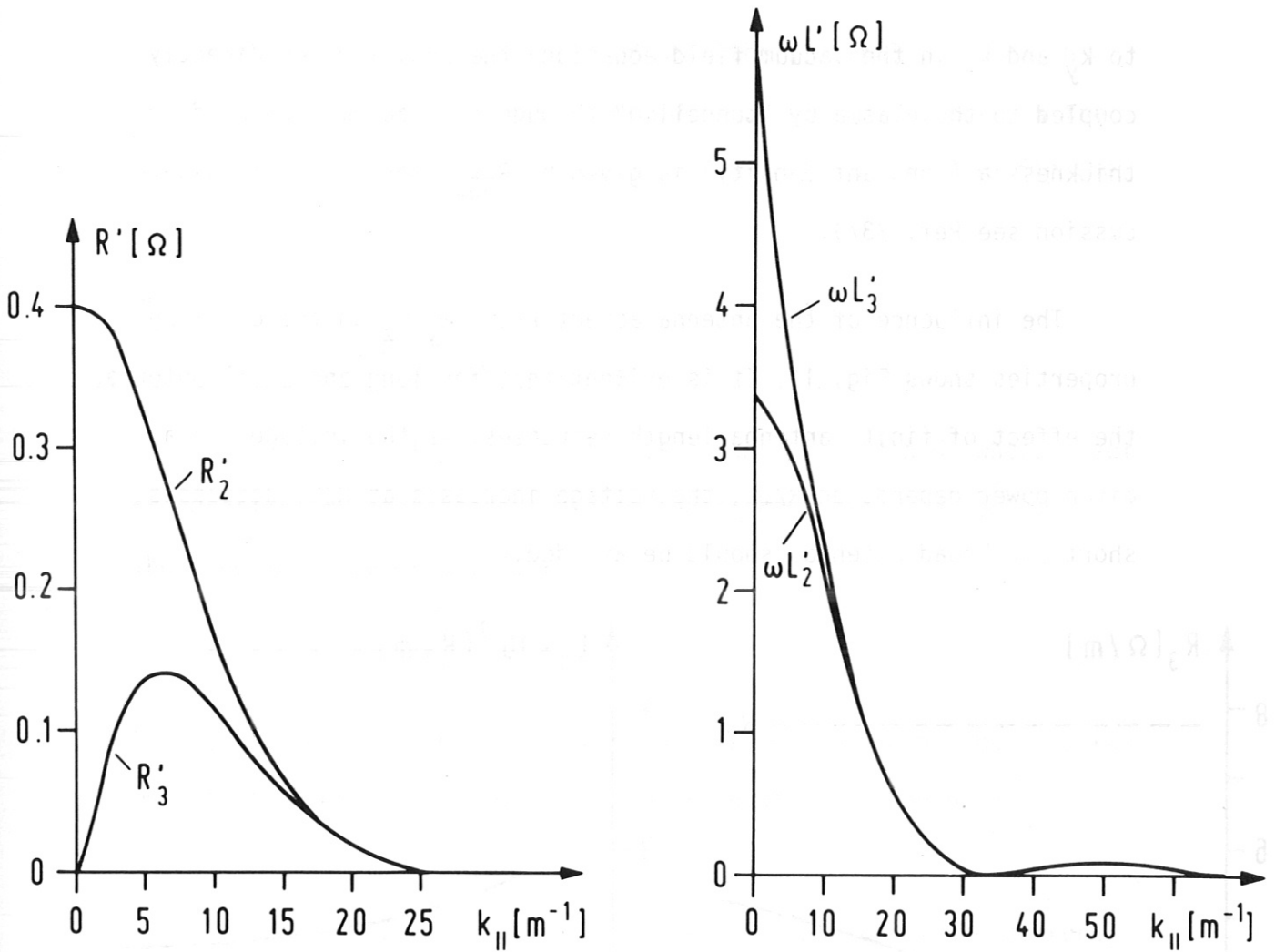$$L_2 = 2.1 \times 10^{-7}\ H/m$$

$$L_3 = 2.5 \times 10^{-7}\ H/m$$

Fig. 10   Spectral functions of the specific resistivity (a) and in-
ductance integrated over k_y from the 3-D_{QS} model and 2-D model
(w_z = 0.09 m, w_y = 0.24 m, a = b = 0.07 m, d = 0.07 m,
n_o = 5 $\cdot$ 10^{19} m^{-3}, f = 70 MHz; ASDEX parameter,
see Sect. IV).

These values demonstrate the influence of the feeders and of k_y,
which decrease the coupling. The changes with respect to the 2-D case
are predominantely at low $k_{\shortparallel}$. This can be understood from the
appearance of k_y in the parameter $p = \sqrt{k_y^2 + k_{\shortparallel}^2}$, which also dominates
the field evancence between antenna and plasma and which decreases
like exp{-2 pa}. In the sense that vacuum radiation is not taken into
account in the 3-D_{QS} limit ($\beta = \sqrt{L \cdot C} \equiv 0$, k_o neglected with respect

to k_y and $k_\parallel$ in the vacuum field equation) the active power directly coupled to the plasma by "tunneling" through the vacuum larger of thickness a (constant density) is given by R_{3QS} (for a further discussion see Ref. /3/).

The influence of the antenna aspect ratio w_y/w_z on the coupling properties shows Fig. 11. It is evident that for long and small antennas the effect of finite antenna length decreases. As the voltage for a given power depends on $R/\omega L$, the voltage increases as $R/L\omega$ decreases, short and broad antennas should be avoided.
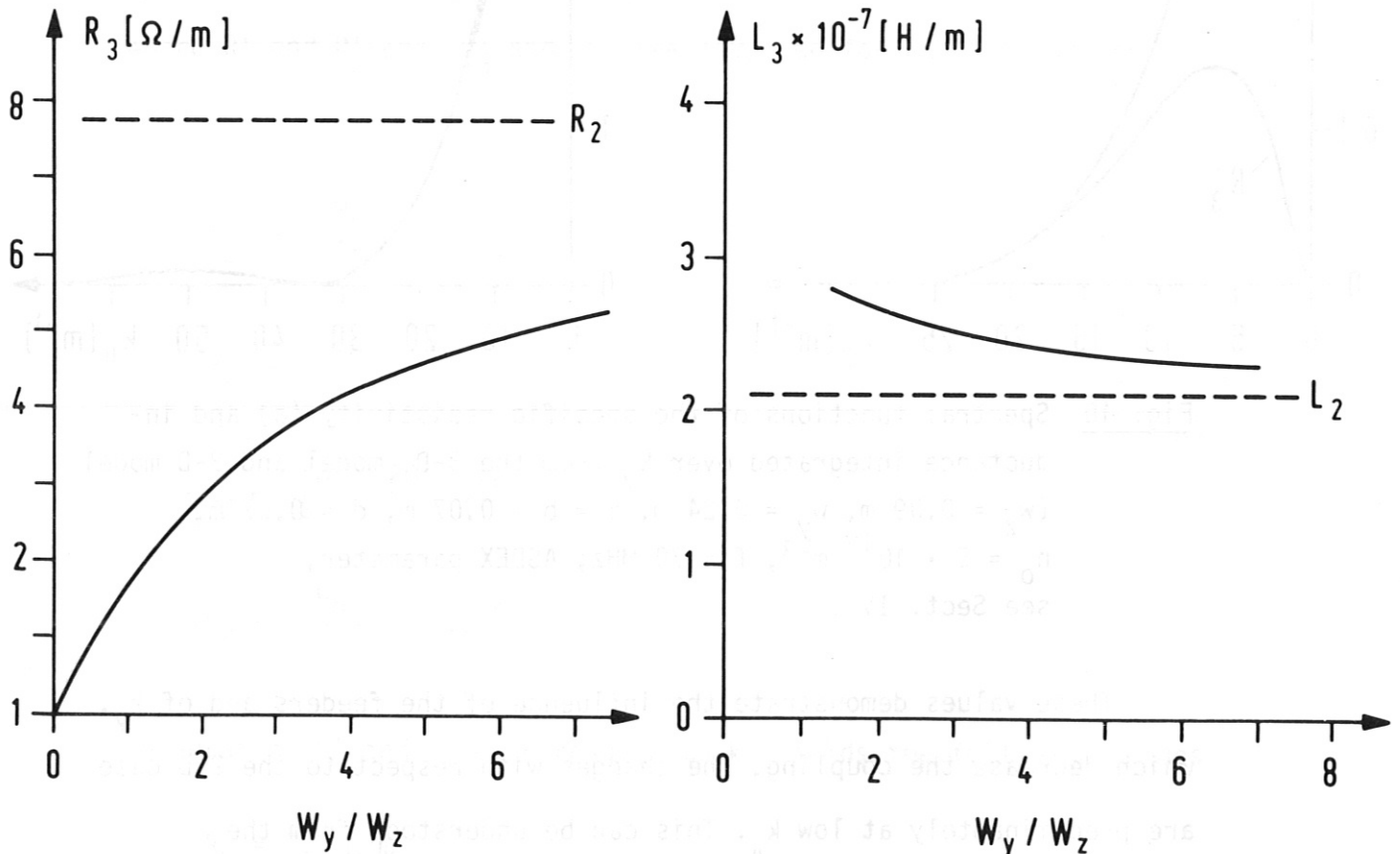

Fig. 11   Specific resistance and inductance versus the antenna aspect ratio w_y/w_z. R_2 and L_2 are the values calculated by the 2-D model (data: see Fig. 10) assuming a step density profile.

Finally it should be mentioned that the spectral functions G'
or R_3' for the active radiated power coupled into the plasma has the
maximum at $k_"$ values above $k_" = 0$ which would be favourable for the
power absorption.

Selfconsistent 3-D Program BARBAR /7/

The variational principle relies on the Ritz method, where a set
of functions is used to approximate the current distribution J.
The functions are of the form:

$$\phi_N = \Sigma \, a_n \cos n\beta y \tag{69}$$

The coefficients of the basis function are determined by the require-
ment that an expression for the antenna input impedance be an
extremum.

Some basic approximations have been made as far as the current
distribution is concerned: the current distribution in the toroidal
direction is taken as square, and the currents flowing in the toroidal
direction on the surface of the conductors have been neglected.

The model of the plasma is simplified by considering cold plasma
dispersion, single pass absorption and coupling to the fast wave only.
The problem of the Lower-Hybrid Resonance which can occur right at the
plasma surface is avoided by assuming a finite plasma density.

The program BARBAR developped by Theilhaber and Jacquinot calcu-
lates the antenna input impedance, current distribution on the central
conductor, electromagnetic field component H_z, E_y, E_x and the pointing
flux S_x (the directions x, y, z are the same as indicated in the
Figures 1, 2, 3).

III. Description of the Computer Programs

A short description of the antenna computer programs, as far as the input and output is concerned, is given in this section.

1. 2-D Program

In Table II the list of the input data is given. The numbers

```
ICRH-Antennen: ASDEX

A         (cm)    =   7.00        (Zentralleiter : Plasmarand)
B         (cm)    =  27.00        (Zentralleiter : Plasma bei Dichtemaximum)
D         (cm)    =   6.90        (Zentralleiter : Vakuumgefäß)
F       (1/sec)   =   7.00  D+07  (Frequenz)
YL        (cm)    =  49.00        (Antennenlänge)
N                 =   2           (Antennenzahl)
W         (cm)    =   9.00        (halbe Antennenbreite)
S         (cm)    =   1.40        (Zentralleiter : Abschirm.-vert)
P         (cm)    =   4.00        (Zentralleiter : Abschirm.-horiz)
RO        (cm)    = 146.00        (Torusachse    : Plasmaradius)
DNO    (1/cm**3)  =   5.00  D+13  (maximale Ionendichte)
RMI               =   1.00        (Atomgewicht)
OMEG              =   2.00        (Omega/Omega-C)
CPO      (1/cm)   =   1.20        (maximal zulässiger Wellenvektor)
DC        (cm)    =   5.90        (Dicke des kapazitiven Belages)
FL        (cm)    =   6.90        (Zentralleiter : Rückleiter)
PE        (MW)    =   0.75        (abgestrahlte Leistung pro Antenne)
GAM               =  -1.00        (Gamma)
JCD               =   1           (=1: J konstant)
                                  (=2: J variabel)
```

Table II: Input list for the 2-D antenna program

correspond to the ASDEX antenna and ASDEX plasma configuration. The symbols used are: A is the distance between central conductor and plasma edge, B is the distance between central conductor and the location, where the plasma density reaches the maximum value (see Fig. 2), D is the distance between central conductor and vessel, F is the operating frequency, YL is the antenna length, N is the number of antennas placed into the torus, W is the half width of the antenna, S is the radial distance between central conductor and Faraday screen, P is the toroidal distance between the edge of the central conductor

and lateral part of the Faraday screen, RO is the major plasma radius, DNO is the maximum plasma density, RMI is the atomic number of the ions, OMEG is the ratio between the operating frequency and ion cyclotron frequency, CPO is the maximum $k_{\shortparallel}$ vector, DC is the radial thickness of the internal capacitance (in the example of Table II the distance between central conductor and upper surface of the internal capacitance, which is mounted on the return conductor is 1 cm), FL is the distance between central conductor and return conductor, PE is the effective radiated power, GAM describes the direction of the current in the return conductor with respect to the direction of the current in the central conductor. GAM = 1 means that the currents flow in the same directions, GAM = -1 in the opposite. The sign of the input parameter is meaningless if D = FL (return conductor is integrated into the vessel). With the input parameter JCD the current density profile in the central conductor is determined; if JCD = 1 a constant current density is assumed, the Fourier transfer given by rel. (17), and if JCD = 2 a current density which is peaked at the central conductor edge (rel.(18)) is assumed.

The main output of the 2-D antenna program is put together in Table III. In the first part the data of parameters are listed which contribute to the calculation of the spectral functions $g'|J|^2$ or $h'|J|^2$ which are symbolized as G(1)SPR and H(1)SPR. The parameters are: $k_{\shortparallel}$ (K-PARALLEL) $= m.n/RO$ (where m is an integer) real- and imaginary part of A (REAL-AK, IMAG-AK), where A is given by the formulas (13), $k_{\underline{i}}^2$ (formula 12), ξ(XI) given by formulas (13) and the real- and

K-PARALLEL	REAL-AK	IMAG-AK	(K-SENK)**2	XI	REAL-ZETA	IMAG-ZETA	J(1/3)		J(-2/3)	
1.000D-03	1.388D-01	0.0	3.853D-01	-5.191D-05	0.0	-3.461D-08	2.508D-03	-1.448D-03	2.790D+04	4.832D+04
1.370D-02	1.387D-01	0.0	3.843D-01	-9.761D-03	0.0	-8.914D-05	3.438D-02	-1.985D-02	1.485D+02	2.572D+02
2.740D-02	1.383D-01	0.0	3.815D-01	-3.927D-02	0.0	-7.173D-04	6.890D-02	-3.978D-02	3.697D-01	6.404D+01
4.110D-02	1.376D-01	0.0	3.769D-01	-8.922D-02	0.0	-2.444D-03	1.037D-01	-5.987D-02	1.633D+01	2.828D+01

```
F1...F10,F14,F16 = ( 3.482D+02  -2.010D+02  (-4.624D-08  -2.670D-08  ( 1.807D-05  -1.043D-05)  ( 1.782D+00   1.029D+00)
                   ( 0.0        -4.936D+02) ( 0.0         7.591D+02)  (-3.085D+02  -5.386D+02)  ( 9.676D-01   0.0      )
                   (-1.874D-01   0.0      ) (-4.970D-01  -8.677D-01)  ( 9.447D+01   1.684D+02)  (-8.566D+01  -4.058D+01)
```

Part 1

K-PAR	STROMPROFIL	G(1)*SPR	H(1)*SPR
1	0.0010	1.0000	-7.402D-01	-4.206D+00
2	0.0137	0.9949	-7.257D-01	-4.170D+00
3	0.0274	0.9799	-6.837D-01	-4.061D+00
4	0.0411	0.9552	-6.189D-01	-3.887D+00

Part 2

Table III

Output of the 2-D antenna program

```
ZOS  = 2.808D+01
ALFA = 1.984D-03
BETA = 3.500D-02      (2*BETA*YL)
                        3.430
R    = 1.114D-01
L    = 2.235D-09
C    = 2.834D-12
VA   = 0.0
VM   = 2.173D+04
ZIN  = 8.363D+01    -1.377D+02
```

Part 3

imaginary part of ζ (REAL-ZETA, IMAG-ZETA), with $\zeta = 2/3 \cdot A \cdot \xi^{3/2}$.
ζ is the argument of the Bessel-Functions $J_{1/3}(\zeta)$ and $J_{-1/3}(\zeta)$. For
$k_\parallel = 0.001$ the functions values F1...F10, F14, F16 which are described
in Appendix I are given; both the real- and imaginary part are listed.

The second part of the output lists $k_\parallel$, $|J|^2$ and the spectral
function $g'|J|^2$ and $h'|J|^2$. $|J|^2$ is named as STROMPROFIL.

The third part lists the main results of the 2-D antenna
program.

$$ZOS = \sqrt{L/C}$$
$$ALFA = R/(2\sqrt{L/C}) \tag{70}$$
$$BETA = \omega\sqrt{L \cdot C}$$

R, L, C are the specific resistivity, inductivity and capacitance
(per cm), V_A and V_M are the antenna input voltage and the maximum
voltage in the antenna if the antenna is longer than $\lambda/4$ (see
formulas 48, 49) and ZIN is the antenna input impedance (46).

2. The 3-D$_{QS}$ Program

The list of the input data and a characteristic section of the
output list is given in Table IV.

The input data are: B is the magnetic induction value at the plasma
centre, A is the distance between central conductor and return con-
ductor (in meters; in 2-D model the geometric dimensions are in cm),
D is the distance between central conductor and return conductor,
F is the frequency, DNO is the plasma density, RMI is the mass number,
Z is the atomic charge number, WZ and WY are the half width and half
length of the central conductor, JCD characterizes the current density

ICRH-Antennen : ASDEX

B	(T)	=	2.29	(Magnetfeld)
A	(m)	=	0.0700	(Zentralleiter : Plasma)
D	(m)	=	0.0690	(Zentralleiter : Rückleiter)
F	(1/sec)	=	7,000E+07	(Frequenz)
BETA	(1/m)	=	0.9800	(Wellenvektor)
DNO	(1/m**3)	=	5.000E+19	(Ionendichte)
RMI		=	1.00	(Atomgewicht)
Z		=	1.00	(Ladung)
WZ	(m)	=	0.0900	(halbe Antennenbreite)
WY	(m)	=	0.2450	(halbe Antennenlänge)
JCD		=	1	(zur Auswahl des Stromprofils)
KPARM	(/m)	=	60.00	(maximales K-Parallel)
NKPAR		=	200	
KYM	(/m)	=	60.00	(maximales K-Y)
NKY		=	200	

```
R-  KPAR,JS12,GS,R3S = -60.000   0.0205   0.000E+00   0.000000
R-  KPAR,JS12,GS,R3S = -59.397   0.0227   0.000E+00   0.000000

        INTEGRAL,R3  =  3.991E-02   3.511E+00
```

Table IV Input data and an output section of the 3-D_{QS} antenna program

profile (see description of the 2-D program), KPARM and KYM are the maximum $k_\parallel$- and k_y values, NKPAR and NKY define the increment between two $k_\parallel$ and k_y values $\Delta k_\parallel$ = 2KPARM/(NKPAR-1) and Δk_y = 2KYM/(NKY-1).

The output lists are organized as follows: the first column gives $k_\parallel$, the second $(\frac{\sin k_\parallel w_z}{k_\parallel w_z})^2$, the third g'_3 (real part of rel. (57) and R'_3(R3S). R'_3 is the spectral function of the resistivity part and is given by (68). Integrating R'_3 with respect to $k_\parallel$ gives R_3; the value of R_3 is listed at the end of the columns which were cutted off in Table IV at $k_\parallel$ = - 59.397. The list for the inductive part (calculation of L_3) were arranged in the same manner as for R_3.

3. 3-D Program BARBAR

The 3-D antenna computer program developed at Fontenay-aux-Roses /7/ was implemented at our institute.

A short description of the input parameters as far as it is necessary for the application of the program is given.

$$\text{MENU} = \left\{ \begin{array}{l} 1 \\ 2 \\ 3 \end{array} \right.$$

1: Calculation for a single frequency with possibly the field structure

2: Calculation for a list of frequencies (DATA 66), with no field structure

3: Same as 2, but adds a convergence estimate.

$$\text{NHOM} = \left\{ \begin{array}{l} 0 \\ 1 \\ 2 \end{array} \right.$$

0: Impedance calculation for an inhomogeneous plasma (and maybe field structure)

1: Calculation for a homogeneous plasma (no field structure)

2: Calculation for the vacuum case.

$$\text{NANT} = \left\{ \begin{array}{l} 1 \\ 2 \end{array} \right.$$

1: One antenna system (sickle antenna)

2: Two antenna systems (antenna pair in our nomenclature)

MUP: Number of trial functions used in the Ritz Method.
       A typical value is 4.

NINC: Number of points skipped in the n_y mesh, in the evaluation of the spectral admittance. The points inside each interval of the ninc points are reached by interpolation.
       A typical value is 10.

NHZ

NEY

NSX = { 0 or 1

NEX

> Each field component and the component of the pointing vector S_x can be suppressed (number 0) or calculated (number 1) individually. Note: for field calculation MENU = 1.
>
> 0: no field calculation
>
> 1: field calculation at (x = RRSTOP,Y,Z) H_z, E_y, Pointing flux SX, E_x; (NSUR = 1 yields E_x calculation at the wall).
>
> The fields are calculated at a distance RRSTOP from the plasma edge; RRSTOP in meters. The field values are calculated at two slices (in the space) forming a cross; one section is for z = 0 and the other is for y = 0.

FREQ: operating frequency

PPN10:   density at the plasma edge in 10^{14} cm^{-3}

PPNO: center plasma density in 10^{14} cm^{-3}

PPBO: magnetic field at the antenna in T

PPRH = n_H/n_e: fraction of hydrogen in the plasma

PPRD = n_D/n_e: fraction of deuterium

RRO: plasma radius (amount of linear profile to reach PPNO), in meters

PPB: distance central conductor - wall, in meters

PPC: distance Faraday screen - wall, in meters

PPD: distance plasma - wall, in meters

PPHA: length of an antenna element, in meters

PPWA: width of the antenna, in meters

FNYMAX: maximum k_y-value

FNZMAX: maximum k_z-value

PPE: distance between wall and internal (or additional) capacitance. In contradiction to Fig. 3, where the internal capacitance is placed on the wall (or on the return conductor), the additional capacitance is in this work fixed on the central conductor (see Fig. 1 /7/).

IV. Some Results

The antenna programmes described in Sections II and III are applied to the operating and planned plasma experiments at IPP Garching; some results are summarized in the following.

1. ASDEX

The geometrical input data used for the calculations are (see also Table II):

Distance central conductor - return conductor	6.9 cm
Distance central conductor - Faraday screen	1.4 cm
Distance central conductor - plasma boundary	7.0 cm
Plasma profile length	20.0 cm
Length of the central conductor	49.0 cm
Width of the central conductor	18.0 cm
Distance between central conductor and additional capacitance	1.0 cm.

2-D calculations

The main ICRH heating scheme is first harmonic of hydrogen,
which for a magnetic induction value at the plasma centre of 2.29 T
corresponds to 70 MHz. The maximum plasma density at the centre is
approximated in the calculation by a value of $5 \cdot 10^{13}$ cm^{-3}.

As second heating scheme hydrogen minority in deuterium
is foreseen. In the 2-D calculation this scheme is approximated as
far as the plasma description is concerned by setting $f = 2 \, f_{CD}$ with
$f = 35$ MHz (RMI = 2; OMEG = 2; see Table II). The results shown in
the following tables and figures are obtained with a constant current
profile: JCD = 1. Changing the current profile JCD = 2 has no sig-
nificant influence on the results /36/.
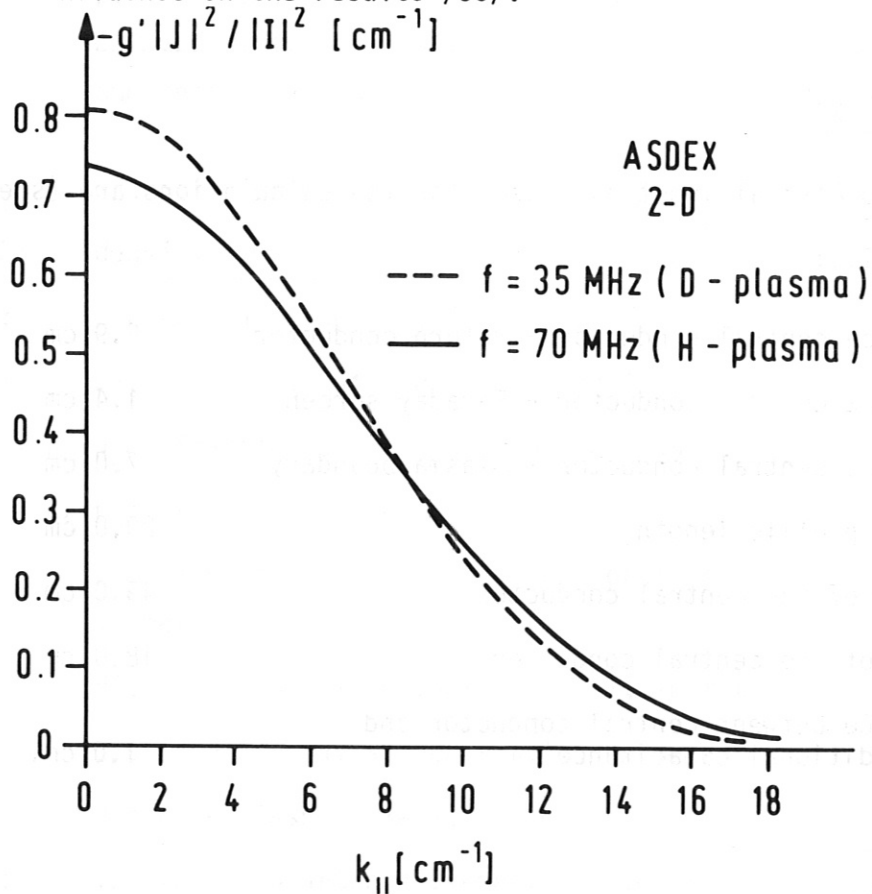
Fig. 12 Spectral functions of the radiated power as a function of $k_{\parallel}$
for ASDEX (calculation carried out with 2-D program)

The spectral functions of the effective radiated power as a function of $k_{\parallel}$ is plotted in Fig. 12 for the two heating schemes, for the first harmonic heating of hydrogen (f = 70 MHz) and for the hydrogen minority heating in a bulk deuterium plasma. The main results are listed in Table V where the antenna parameters for the two scenarios are collected. The radiated power of each antenna is 750 KW corresponding to 1.5 MW for one antenna pair. The total ASDEX antenna system consists of 2 antenna pairs (see Refs. /24, 25/). The antenna data are calculated for a plasma density in the centre of $5 \cdot 10^{13}$ cm^{-3}.

	1. harmonic of hydrogen; f = 70 MHz	Minority heating f = 35 MHz
R [Ω/m]	11.14	5.78
L [H/m] $\cdot 10^{-7}$	2.24 +)	2.32
C [F/m] $\cdot 10^{-10}$	2.83	2.83
V_A or V_M* [kV]	21.7	18.0
Zin [Ω]	83.63 - j 137.7	5.33 + j 33.67
Q = ωL/R	8.8	8.8
V_{max} [kV]**, *	21.85	24.1
2 β ℓ	3.43	1.75

*   750 kW radiated power for each antenna

**   on a 30Ω-line

+)   The L value of $2.24 \cdot 10^{-7}$ H/m is about 50 % of the value of strip transmission line in vacuum.

Table V ASDEX antenna data calculated with the 2-D program; internal or additional capacitance is included (geometrical data see page 35). Plasma density $n_0 = 5 \cdot 10^{13}$ cm^{-3}
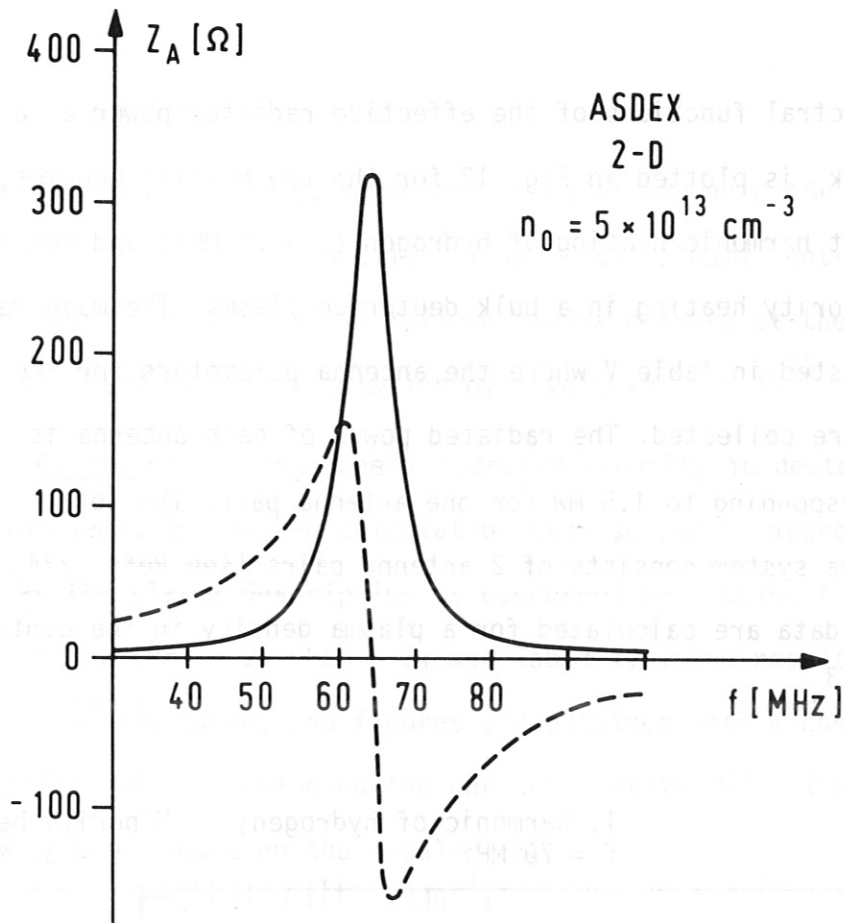
Fig. 13 Real (———) and imaginary (----) part of the input
         impedance for an ASDEX antenna (geometrical data see
         page 35)

At an operating frequency of 70 MHz the antenna section is
longer than $\lambda/4$. The resonant frequency, as can be seen from Fig. 13,
where the antenna input impedance as plotted versus the frequency
($2\omega_r \sqrt{L \cdot C} \cdot \ell = \pi$; ℓ is the antenna length) is 64.1 MHz.   The
voltages in the antenna V_M or V_A are 21.7 or 18 kV.

The maximum voltages V_{max} on a 30 Ω line which follow from the
antenna input impedance are given in Fig. 14 (using rel. 50, 51).

One antenna pair installed into the ASDEX vessel is without an
additional capacitance. This has consequences on the electrical length
and therefore on the antenna input impedance. Table VI shows the main
parameters for such antenna (DC = 0).
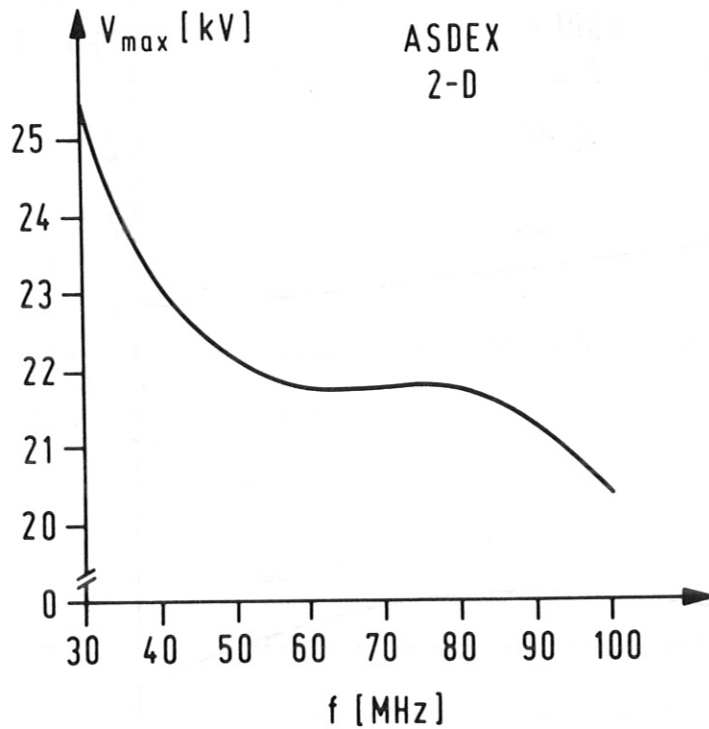
Fig. 14

Maximum voltages on a
30 Ω line which follow
from the antenna input
impedance of Fig. 13

	1. Harmonic of hydrogen f = 70 MHz	Minority Heating f = 35 MHz
C [F/m]	$1.5 \cdot 10^{-10}$	$1.5 \cdot 10^{-10}$
V_A [kV]	24.34	18.12
VSWR	14.12	15.21
V_{max} [kV]	25.2	26.2
2 β ℓ	2.50	1.27
Z_{in} [Ω]	32.3 + j 108.7	3.8 + j 28.77

Table VI ASDEX antenna data calculated with the same parameters
as for Table V, but without additional capacitance.

The resonance frequency increases to 88 MHz; the maximum voltage
on the 30 Ω line and the voltages in the antenna increases also.
For f = 70 MHz the voltage increases from 21.85 kV to 25.2 kV
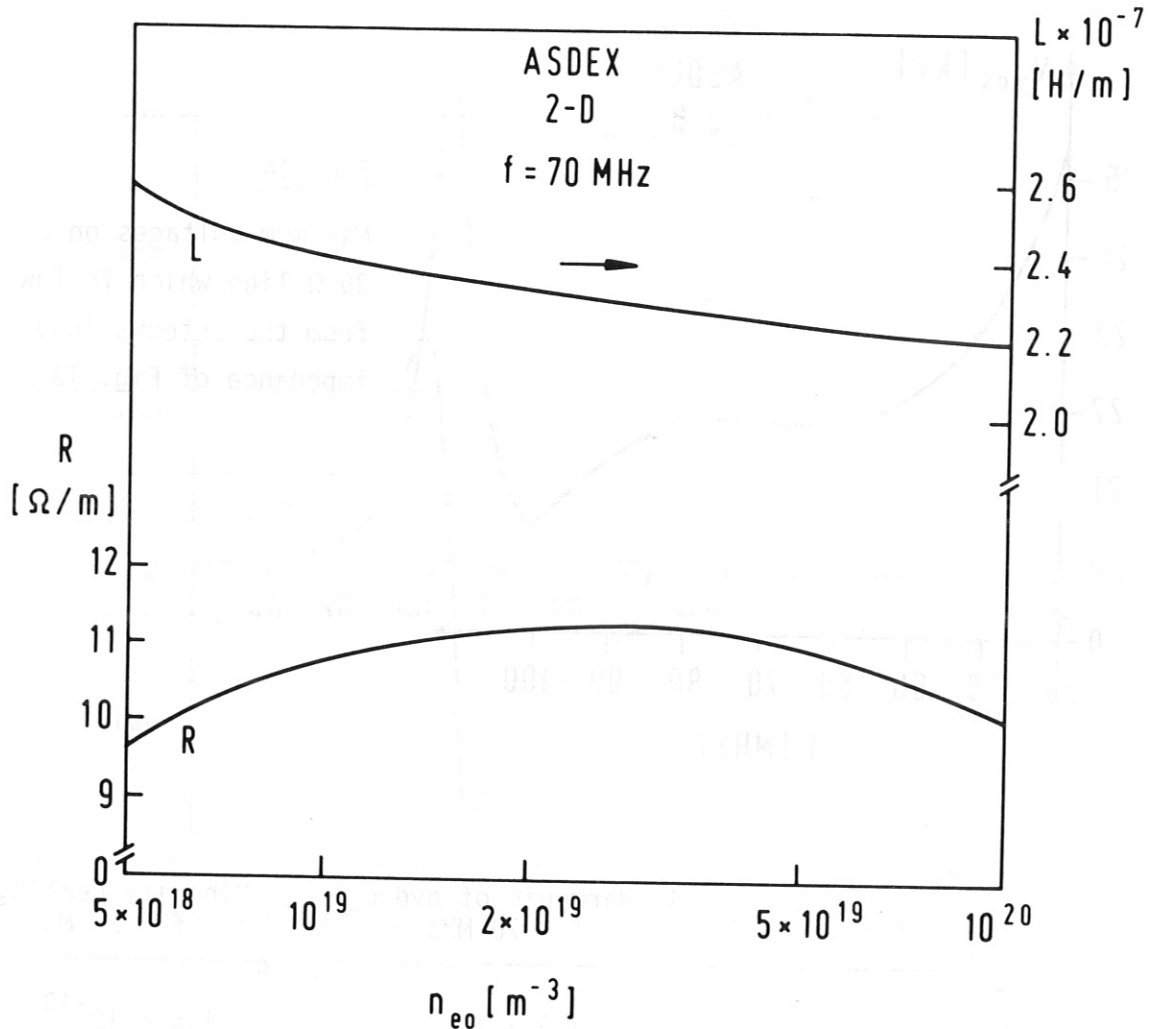
Fig. 15   Variation of R and L of the ASDEX antenna with the central plasma density

Using the 2-D calculations we have investigated the dependence of the coupling properties R and L on the central plasma density n_{eo} (DNO). This is shown in Fig. 15. The dependence of R and L on n_{eo} in the range between $5 \cdot 10^{18}$ and 10^{20} m^{-3} is rather weak as shown in Fig. 15.

The specific impedance L of the plasma increases for the vacuum case to $2.7 \cdot 10^{-7}$ H/m. The resonance frequency in vacuum is related to the resonant frequency with plasma (in the 2-D model) according to

$$\frac{f \text{ res (without plas.)}}{f \text{ res (with plas.)}} = \left\{\frac{L \text{ (with plas.)}}{L \text{ (without plas.)}}\right\}^{1/2} \tag{71}$$

This corresponds to 58 MHz for the vacuum case (64 MHz with plasma).

3-D$_{QS}$ calculations

As discussed in Section III, the influence of the feeders decreases R and increases L. For an ASDEX antenna and $n_{eo} = 5 \cdot 10^{19}$ the 3-D$_{QS}$ values are:

$$R_{QS} = 3.5 \ \Omega/m$$
$$L_{QS} = 2.5 \cdot 10^{-7} \ H/m$$

The corresponding 2-D values are (see Table V) 11.14 Ω/m and $2.24 \cdot 10^{-7}$ H/m. (The R_2 value of page 26 was calculated under the assumption that the plasma density is constant over the plasma cross-section, which yields lower R_2 values than when an inhomogeneous plasma is taken into account.)

3-D calculations

3-D calculations were also carried out with the computer program BARBAR /7/.

For a pure hydrogen plasma and a deuterium plasma with 5 % hydrogen the antenna input impedance curves are shown in Figs. 16 and 17 (note that the imaginary is the negative in comparison to that of Fig. 13, because the time dependence in BARBAR is $e^{i\omega t}$ instead of $e^{-i\omega t}$ used in the 2-D model).

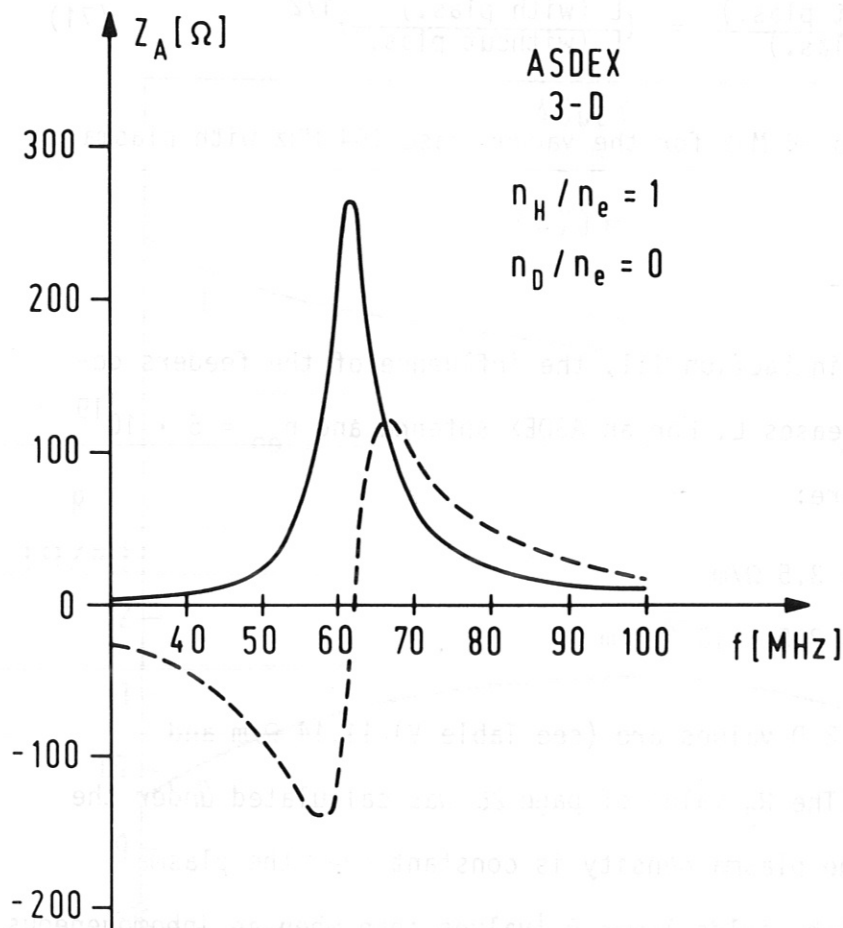The antenna data are calculated with an edge plasma density of 10^{12} cm^{-3} (PPN10 = 10^{-2}).

Fig. 16

Antenna input impedance Z_A versus frequency for an ASDEX antenna with additional capacitance (hydrogen plasma $n_H/n_e = 1$; $n_D = 0$).
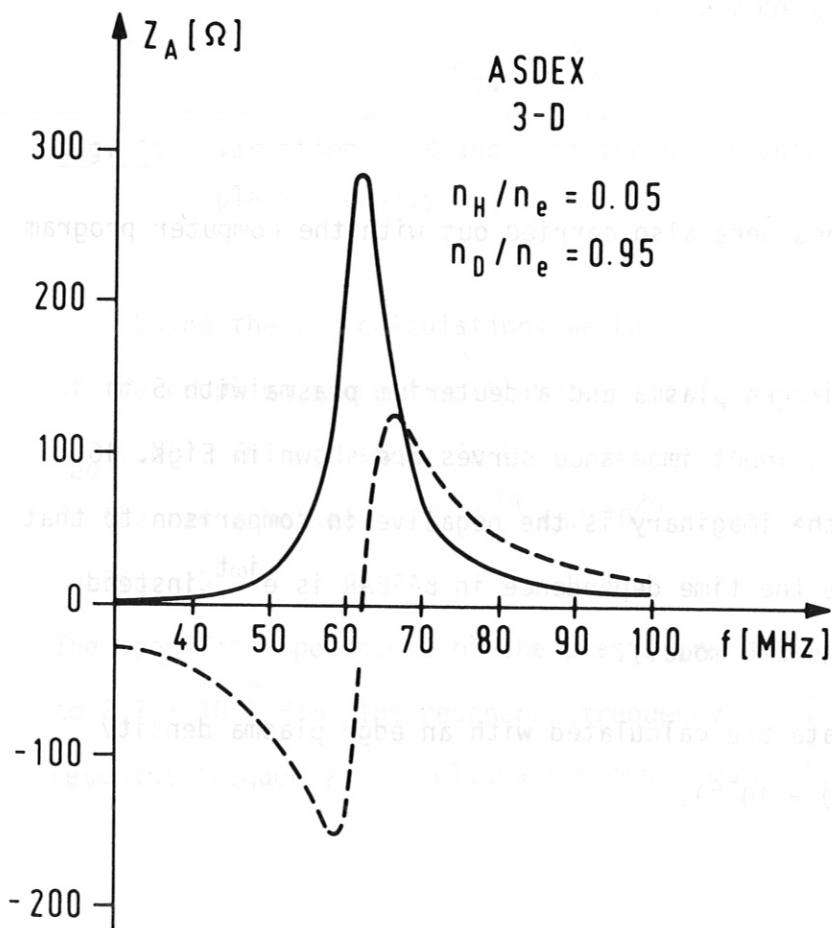
——— real part

---- imaginary part

Fig. 17

Antenna input impedance Z_A versus frequency for an ASDEX antenna with additional capacitance (deuterium plasma with 5 % hydrogen)

——— real part

---- imaginary part

Besides small deviations in the region of the resonance frequency (f_{res} = 63 MHz) the curves of Figs. 16 and 17 are nearly identical. These computations confirm the results already obtained by 2-D and 3-D calculations, /3, 5, 7, 8/ that the antenna propagation constant is principially determined by the antenna dimensions and is largely unaffected by the plasma properties.

The maximum voltages on a 30 Ω line calculated with formulae (50) and (51) from Z_A of Fig. 16 are shown in Fig. 18.
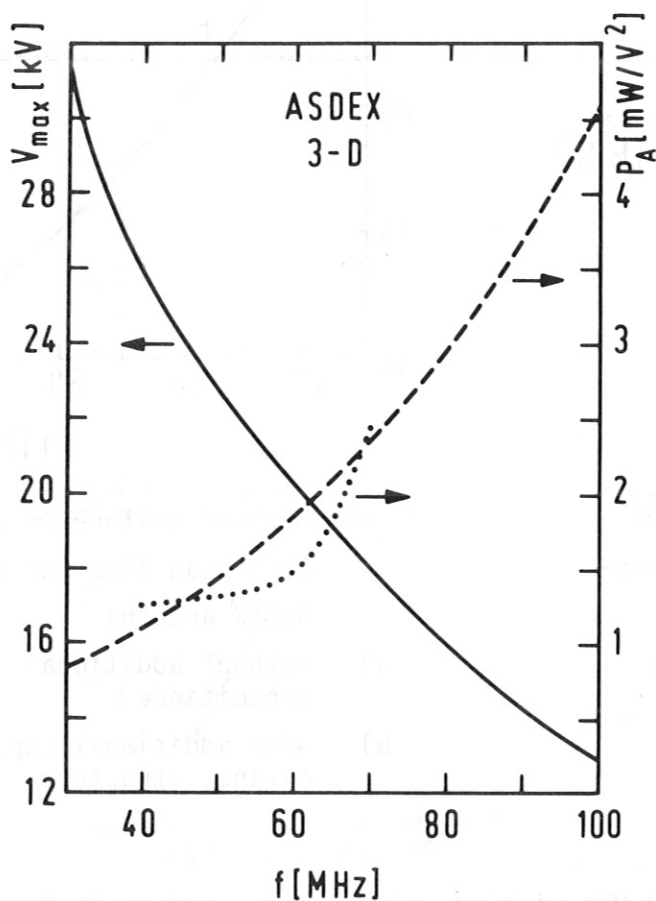
Fig. 18
Maximum voltage V_{max} on a 30 Ω coax line and the normalized input power P_A as used by Puri /8/ versus frequency ($P_A = P/V^2_{max}$). The lined curve (----) follows from Fig. 14 and the dotted one from Puri's work /8/.

In addition to the dependence of V_{max} on f an antenna efficiency curve is shown where $P_A = P/V^2_{max}$ /8/ is plotted versus frequency. The curves show that the antenna improves with increasing frequency.

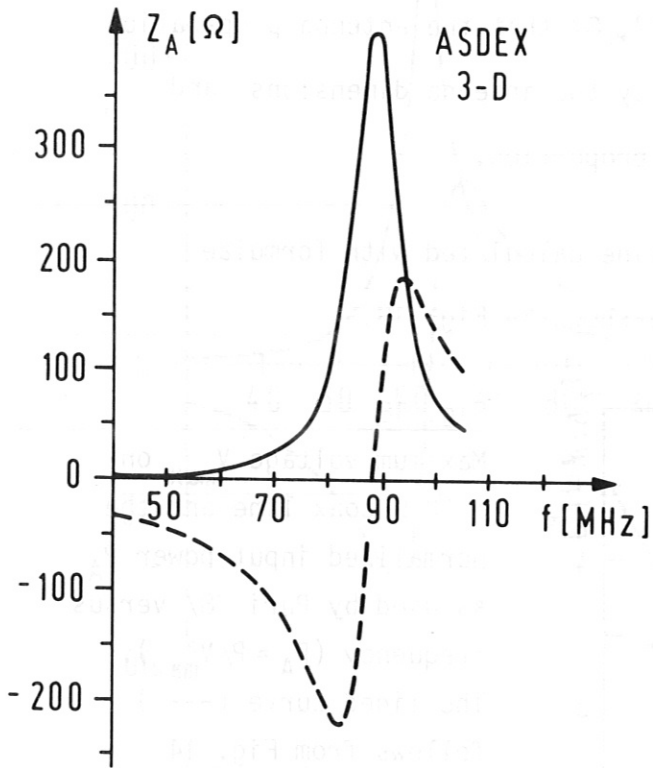The influence of additional capacitance is discussed in connection with Figs. 19 and 20.

Fig. 19 ASDEX antenna input
impedance versus fre-
quency.
The antenna has no
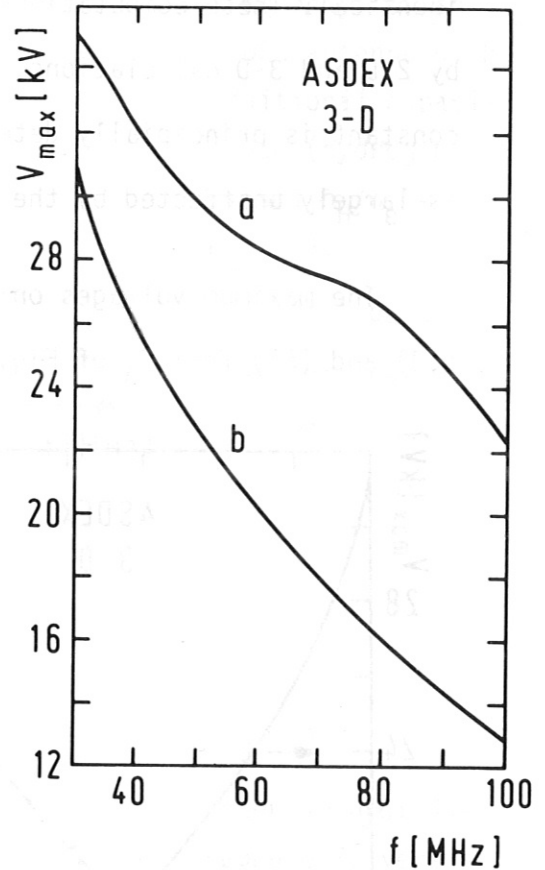additional capacitance
structure

Fig. 20 Maximum voltage on a
30 Ω coax line for an
ASDEX antenna
a) without additional
capacitance
b) with additional capa-
citance structure

The resonance frequency (63 MHz with additional capacitance) increases without additional capacitance to 87 MHz (2-D calculations = f_{res} = 88 MHz). The maximum voltages on a 30 Ω line are for the antenna without additional capacitance considerably higher, the difference in the maximum voltages between an ASDEX antenna with and without an additional capacitance is more pronounced in the 3-D calculation than in the 2-D calculations.

The current distribution of the capacitively loaded ASDEX
antenna is shown in Fig. 21 for the two main operating frequencies
35 and 70 MHz. (Calculations are carried out with the computer
program BARBAR /7/.) At 70 MHz the antenna input current I_A is nearly
minimum thus reducing E_x-fields and the power P_s going into the waves
travelling between the wall and plasma surface (coax modes) which may
be responsible for impurity production. The power P_s which scales like
$|I_A|^2$ /7/ is reduced. At the operating frequency of 35 MHz the
situation is as far as the I_A value is concerned is more critical. The
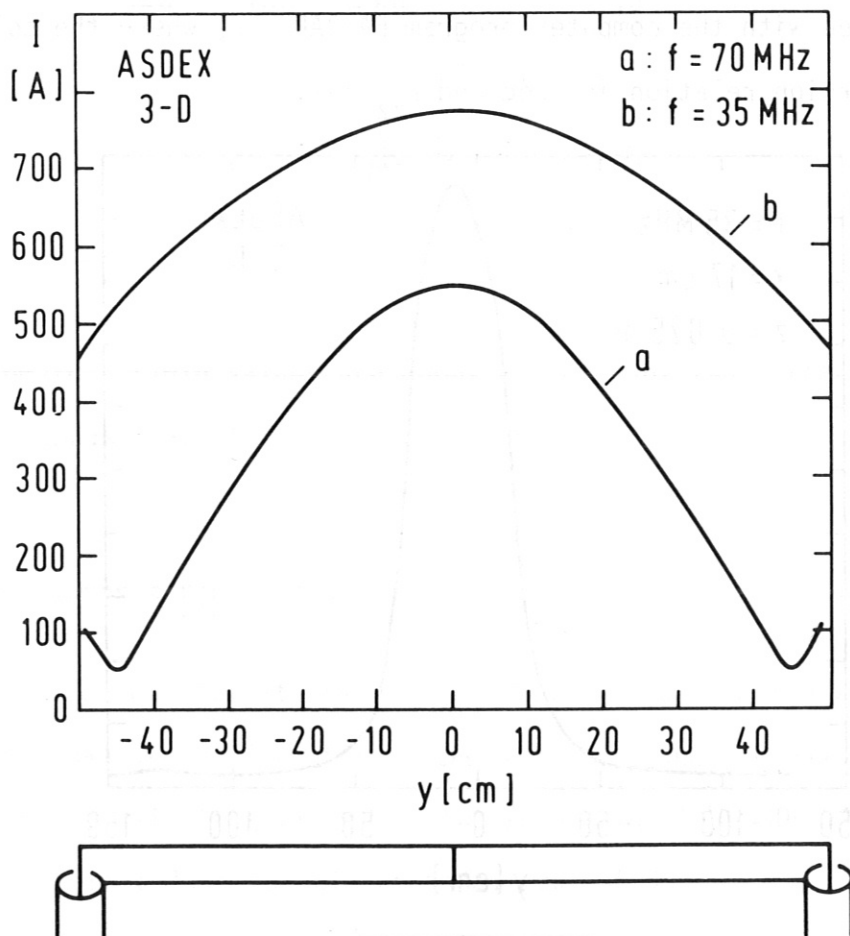ratio I_A (f = 35 MHz)/I_A(f = 70 MHz) is about 5 ($P_s \propto |I_A|^2$!).

Fig. 21 Current distribution of the capacitively-loaded ASDEX
antenna for the two main operating frequencies 35 and
70 MHz.

The dispersion relation for such waves is $k_y^2 + k_z^2 = k_o^2$ (k_o^2 for 70 MHz is 2 m^{-2} or 0.5 m^{-2} for 35 MHz). The minimum $k_z = k_{\shortparallel}$ value if one antenna is operating is $k_{\shortparallel\ min} = 1/R_o \cong 0.7$ (assuming that the $k_{\shortparallel} = 0$ mode doesn't really exist) and the minimum k_y value is for ASDEX vessel dimension about 1 m^{-1}. The sum of $k_{y\ min}^2 + k_{\shortparallel min}^2$ is about 1.5 which is larger than k_o^2 at a frequency of 35 MHz. From the dispersion relation follows that propagation of the coax mode at f = 35 MHz around the torus is hindered.

The influence of the higher current on the fields when the antenna is operated at 35 MHz is seen from Figs. 22 and 23. The fields are calculated with the computer program BARBAR /7/, where the cold plasma dispersion relation is used and $K_{zz} \to \infty$.
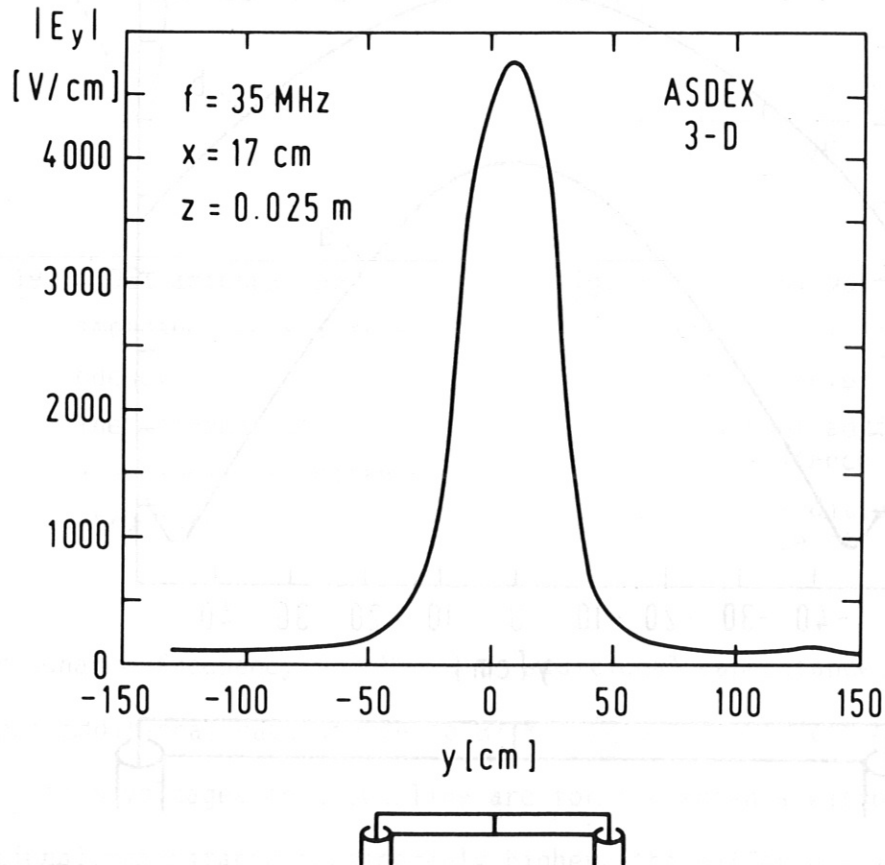

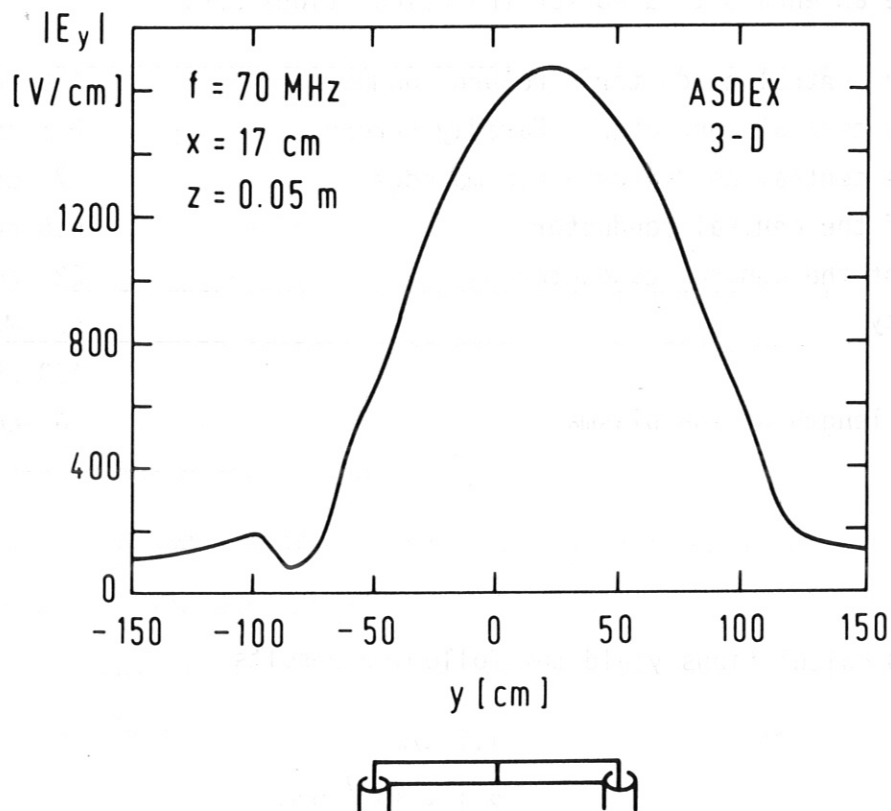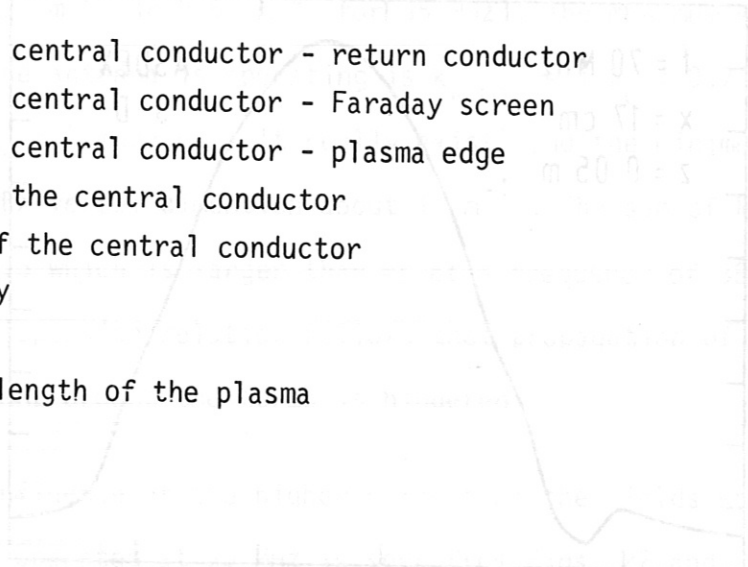Fig. 22 Field inside the plasma (10 cm from the plasma boundary) for f = 35 MHz

Fig. 23   Field inside the plasma for f = 70 MHz

The $|E_x|$ field values are about a factor of two larger for both antennas than the $|E_y|$ value.

2.   WENDELSTEIN   VII-A

The configurations of the W VII-A (and also the W VII-AS) antennae are different from the ASDEX antenna; whereas the ASDEX antenna pair is composed of two antennae, the WENDELSTEIN antennae are sickle-like (single antenna) /25, 45/).

The antenna data used for the calculations are:

Distance central conductor - return conductor	1.6 cm
Distance central conductor - Faraday screen	0.5 cm
Distance central conductor - plasma edge	7 cm
Width of the central conductor	5.6 cm
Length of the central conductor	22 cm
Frequency	50 MHz
Power	100 kW
Profile length of the plasma	6 cm

The <u>2-D</u> calculations yield the following results

R	$1.2 \ \Omega/m$
L	$2.1 \cdot 10^{-7} \ H/m$
C	$1.4 \cdot 10^{-10} \ F/m$
V_A	12.6 kV
V_{max} (on 30 Ω line)	28.5 kV
Z_A	$0.28 + j \ 15.46 \ \Omega$
VSWR (on 30 Ω line)	135

The quality factor defined for a transmission line model is

$Q_{TS} = \omega L/R = 55.$

<u>With the 3-D</u> program (BARBAR) the antenna input impedance is

Z_{in} (Ω) = 0.08 + j 13.8 yielding a VSWR (30 Ω line) of 454 and a

maximum voltage on the 30 Ω coax line of 52 kV.

3. WENDELSTEIN VII-AS

A preliminary design of W VII-AS antenna leads to the following antenna data:

Distance between central conductor and return conductor   6.5 cm

Distance between central conductor and plasma boundary   7.0 cm

Distance between central conductor and Faraday screen   1.0 cm

Length of the central conductor   40 cm

Width of the central conductor   25 cm

Distance between central conductor and additional capacitance   1.0 cm

Radiated power per antenna   750 kW

For the calculations a hydrogen plasma is taken into account.

The main results calculated with the computer program BARBAR /7/
are:

Antenna input impedance at f = 70 MHz   100-j 10 Ω

VSWR   3.75

Maximum voltage on the coax line (Z_c = 30Ω)   13 kV.

The resonance frequency with additional capacitance is 71 MHz and
without 95 MHz.

The main voltage on the 30 Ω line is 13 kV for a radiated power
of 750 kW. Taking into account the experience with coax lines,
higher maximum voltages can be sustained. Reduction of the central
conductor width, increasing the reactive part of antenna impedance,
may be possible. Another possibility would be to use instead of a
broad central conductor a conductor array in order to shape the $k_{\parallel}$
spectrum.

For matching the influence of the plasma density on the antenna input impedance is important. As an example the dependence of Z_A on the plasma density for a W VII-AS antenna without additional capacitance is shown in Fig. 24. The operating frequency is 70 MHz, being 15 MHz below the resonance frequency 85 MHz.
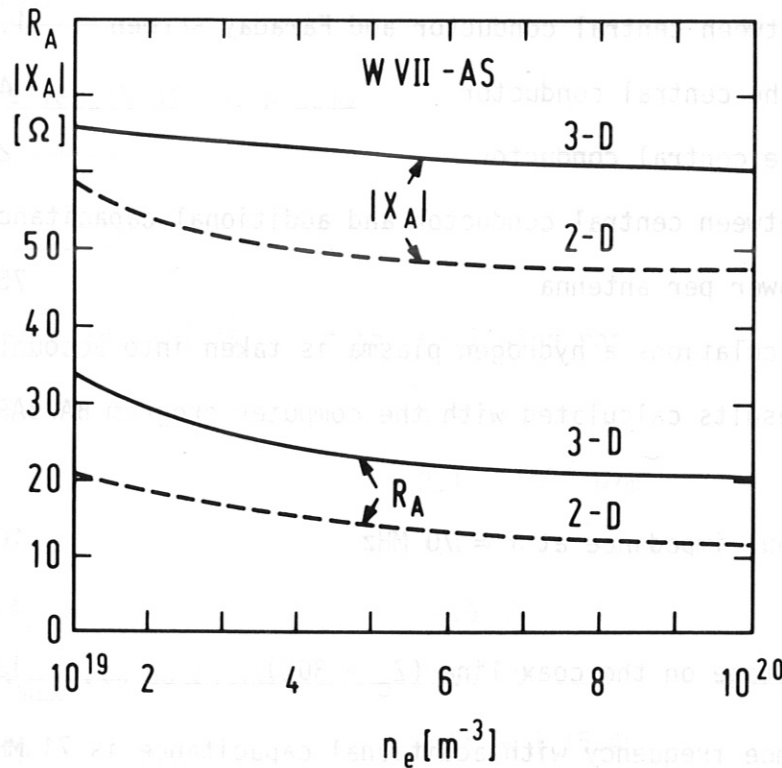

Fig. 24 Dependence of the W VII-AS antenna input impedance versus the plasma density (hydrogen plasma).
The antenna has no additional capacitance.

——— 3-D: BARBAR /7/
---- 2-D:

The variation of R_A and X_A in the investigated density range is small; this is mainly because that the operating frequency and the resonance frequency differ considerably.

The difference between the 2-D and the 3-D results are modest.

4. ASDEX UPGRADE

As can be seen from Figs. 5 , three antenna configurations are possible. The first one, designated as the "normal antenna" (Fig. 5a), shows the geometrical and electrical features of the antennae which have commonly been used up to now for ICRH, and which are envisaged for the ASDEX and W VII systems. The antenna is feed at one end and short-circuited at the other. As a further feature of this antenna type, the distance between the central conductor and return conductor is constant. The disadvantage of this antenna type for ASDEX Upgrade is twofold: firstly, a very complex coax line with two curvatures (see Fig. 5a) has to be established within a short length between the vessel and antenna feeder; secondly, the large distance between the central conductor and vessel is not used. Two other possibilities should be discussed where the distance between the central conductor and vessel is better used. For the first possibility, which is the second configuration (Fig. 5b), the distance between the central conductor and return conductor varies up to the maximum allowable value of about 15 cm. The third antenna configuration is characterized by the fact that the coax line is straight until the antenna input and therefore the antenna is not fed at the geometrical end (see Fig. 5c). As a consequence of the simpler coax arrangement, the maximum distance between the central conductor and vessel would be better used over the total antenna length, as can be seen from Fig. 5c. The question arises whether the antenna part where the currents flow in opposite directions impairs the coupling of the total antenna to the plasma.

One ASDEX Upgrade antenna pair consisting of two antennas (monopole structure) should radiate 1.5 MW; the operating frequencies lie between 80 and 120 MHz corresponding to "1. harmonic hydrogen heating."

As a first step in the ASDEX Upgrade antenna optimization studies the three possible configuration were compared with respect to V_{max} or $P_A = P/V_{max}^2$. The first studies were carried out with antenna configurations without an additional capacitance structure.

For the following calculation the plasma parameters are kept constant; they are:

Distance central conductor and plasma boundary (separatrix)	8 cm
Plasma density in the centre	$2 \cdot 10^{14}$ cm^{-3}
Major plasma radius	165 cm
Profile length of the plasma	20 cm

Frequency: $\omega/\omega_{CH} = 2$

1. Normal antenna

The geometrical data of a normal antenna are:

Length of the central conductor	45 cm
Width of the central conductor	20 cm
Distance central conductor - return conductor	6 cm
Distance central conductor - Faraday screen	1 cm

The main results for a frequency of 80 MHz calculated with the 2-D model are:

R	7.03 Ω/m
L	$1.9 \cdot 10^{-7}$ H/m
C	$2.2 \cdot 10^{-10}$ F/m
$Z_0' = \sqrt{L/C}$	29.3 Ω
$2 \beta \ell$	2.91
V_A (antenna input voltage)	27.2 kV
Z_A	$106 + j\ 203\ \Omega$
V_{max} (30 Ω; P = 750 kW)	27.5 kV

The antenna input impedance curves are shown in Fig. 25. The resonance frequency is 86 MHz.
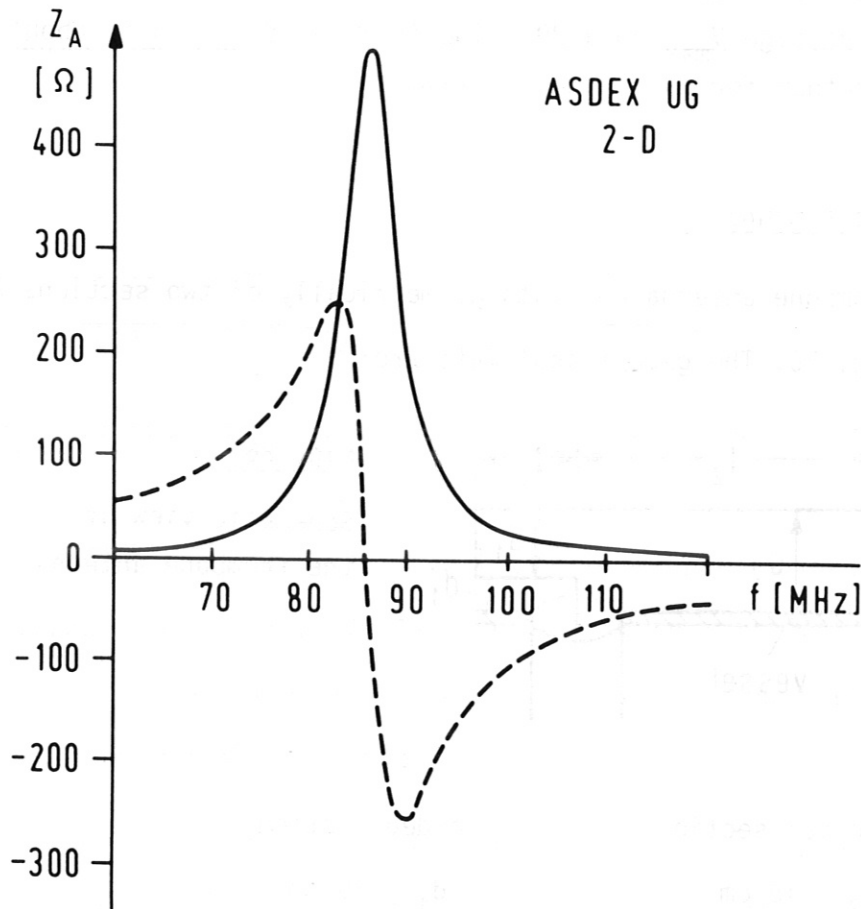
Fig. 25   ASDEX Upgrade antenna input impedance versus frequency
(antenna with no additional capacitance)

b) Step_antenna

The step antenna (see Fig. 6b) is composed from two parts,
one smaller one (length 13.5 cm), where the distance between central
conductor and return conductor is 6 cm, and a larger one (length
31.5 cm), where the corresponding distance is 15 cm.

The main results for the two sections are:

	Small section	Large section
R [Ω/m]	7.05	15.2 Ω/m
L [H/m] · 10^{-7}	1.89	2.63
C [F/m] · 10^{-10}	2.2	2.06
Z_0 [Ω]	29.3	35.6

The input impedance of the step antenna follows from (53):

$Z_A = 142.8 - j\ 157.41\ \Omega$.

The maximum voltage V_{max} on a $30\ \Omega$ line is 21.8 kV, which is about 7 kV smaller than for the normal antenna.

c) Trombone antenna

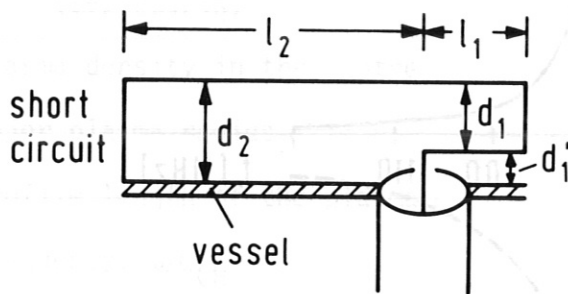The trombone antenna consists geometrically of two sections as shown in Fig. 26. The geometrical data are:

Fig. 26

Schematic view of the trombone antenna

Normal section	Folded section
d_2 = 15 cm	d_1 = 10 cm
ℓ_2 = 31.5 cm	ℓ_1 = 13.5 cm
w = 10 cm	w = 10 cm
s = 1 cm	d_1' = 5 cm
	s = 1 cm

The plasma data are the same as for the normal antenna and for the step antenna (a = 8 cm, b = 28 cm, $n_o = 2 \cdot 10^{14}\ cm^{-3}$). The main difference between the trombone and step antenna as far as the geometry is concerned is that the available space can be used better with the trombone antenna; d_1 is about twice as large for the trombone antenna as the corresponding distance for the step antenna.

The results for a frequency of 80 MHz ($\omega = 2\,\omega_{CH}$) are:

Normal section	Folded section	
	Transmission line mode ($\gamma = 1$)	Antenna mode ($\gamma = + 1$)
$R = 15.23\ \Omega/m$	$7.51\ \Omega/m$	$6.43\ \Omega/m$
$L = 2.62 \cdot 10^{-7}\ H/m$	$3.11 \cdot 10^{-7}\ H/m$	$1.49 \cdot 10^{-7}\ H/m$
$C = 2.06 \cdot 10^{-10}\ F/m$	$2.47 \cdot 10^{-10}\ F/m$	$2.12 \cdot 10^{-10}\ F/m$
$2\beta\ell = 2.33$	$2\beta\ell = 1.189$	$2\beta\ell = 1.52$
$Z_2 = 19.71 + j\ 79.90\ \Omega$	$Z_a = 1.316 + j\ 23.97\ \Omega$	$Z_s = 1.3225 + j\ 69.103\ \Omega$

The input impedance Z for the trombone antenna follows from rel. (55). The maximum voltage on a $30\,\Omega$ line is 18.8 kV (P = 750 KW) which is about 10 kV smaller than the value for a normal antenna and about 3 kV smaller than for the step antenna.

A disadvantage of the folded dipole antennae is a very strong variation of the input impedance versus frequency. In addition this variation is in character different from the input impedance variations of a transmission line (see Figs. 5 - 15(a) and 5 - 15(b) of Ref. 43). Thus the variation of V_{max} versus frequency is larger than for the normal antenna. A detailed study of the frequency de-pendence of Z, V_{max} of trombone antennae (which consists of a folded antenna and a normal antenna) are necessary for application within a frequency range as is foreseen for ASDEX Upgrade. (A discussion of some characteristic features of the folded antenna is given in Appendix I.)

Acknowledgements

Appendix I

2-D Model with Plasma Density Gradient for Folded Antennas

We describe here the formula for the antenna system with return conductor placed before the vessel used in the 2-D computer program; the plasma density is taken into account by a linear density profile between the plasma boundary and the location (input parameter B) where the maximum density is reached (see Fig. 2).

For both conductors, the central conductor and the return conductor, the function $g - ih$ are calculated separately ($g_{21} - ih_{21}$ for the central conductor, $g_{22} - ih_{22}$ for the return conductor(; for the total system $g_2 - ih_2$ is calculated by superposition of the g_{21}, g_{22}, h_{21}, h_{22} functions.

From the functions $g_{21} \ldots h_2$ the R and L values are calculated according the procedure described in Section II.

The geometric functions are:

for the central conductor

$$g_{21} - ih_{21} = \frac{i}{p} \; \frac{e^{-2pd} - 2\gamma C_1 - 1}{F_{16} - 1 - e^{-2pd}(F_{16} + 1)} \tag{A I-1}$$

for the return conductor

$$g_{22} - ih_{22} = \frac{i}{p} \; \gamma C_1 \; \{\frac{-2 \; [1 + C_1\gamma(1 + F_{16})]}{F_{16} - 1 - e^{-2pd}(F_{16} + 1)} + \gamma e^{pr}\} \tag{A I-2}$$

and for the total system

$$g_2 - ih_2 = \{g_{21} + g_{22} + i \; (h_{21} + h_{22})\} \tag{A I-3}$$

In (A I-1) - (A I-3) the following definitions are used:

$$C_1 = (e^{-2pd} e^{pr} - e^{-pr})/2 \qquad \text{(A I-4)}$$

$$F_{16} = \frac{F_{14} (e^{-2pa}+1) + 1-e^{-2pa}}{F_{14} (e^{-2pa}-1) - 1-e^{-2pa}} \qquad \text{(A I-5)}$$

$$F^{14} = \frac{F_1 F_6 F_{10} - F_1 F_7 F_9 - F_2 F_8 F_7 - F_2 F_5 F_{10}}{F_3 F_6 F_{10} - F_3 F_4 F_9 + F_4 F_7 F_8 + F_4 F_5 F_{10}} \qquad \text{(A I-6)}$$

$$F_1 = \frac{i}{k_{\shortparallel}} \xi A J_{-2/3} (\zeta) \Big|_{x=-a} \qquad F_2 = \frac{i}{k_{\shortparallel}} \xi A J_{2/3}(\zeta) \Big|_{x=-a}$$

$$F_3 = -\frac{ip}{k_{\shortparallel}} \xi^{1/2} J_{1/3}(\zeta) \Big|_{x=-a} \qquad F_4 = -\frac{ip}{k_{\shortparallel}} \xi^{1/2} J_{-1/3}(\zeta) \Big|_{x=-a}$$

$$F_5 = \frac{i}{k_{\shortparallel}} \xi A J_{-2/3}(\zeta) \Big|_{x=-b} \qquad F_6 = \frac{i}{k_{\shortparallel}} \xi A J_{2/3}(\zeta) \Big|_{x=-b} \qquad \text{(A I-7)}$$

$$F_7 = \frac{k_{\perp b}}{k_{\shortparallel}} e^{i k_{\perp b} \cdot b} \qquad F_8 = \xi^{1/2} J_{1/3}(\zeta) \Big|_{x=-b}$$

$$F_9 = \xi^{1/2} J_{-1/3}(\zeta) \Big|_{x=-b} \qquad F_{10} = e^{i k_{\perp b} b}$$

For $k_{\shortparallel} > k_{\shortparallel \, max}$ ($k_\perp^2 < 0$) F_7 and F_{10} are changed to

$$F_7 = i \frac{|k_{\perp b}|}{k_{\shortparallel}} e^{-|k_{\perp b}|} \qquad F_{10} = e^{-|k_{\perp b}| \cdot b} \qquad \text{(A I-8)}$$

The functions F_1, F_2, F_3, F_4 are calculated for the conditions at the plasma boundary ($x = -a$) and F_5, F_6, F_8, F_9 at $x = -b$ (see Fig. 2).

The functions A, ξ are defined in Section II by rels. (13); the arguments of the Bessel-Function are

$$\zeta = 2/3 \cdot A \cdot \xi^{3/2} \qquad \qquad \text{(A I-9)}$$

The parameter γ describes the relative direction of the current in the return conductor to the current in the central conductor. $\gamma = 1$ means the currents are parallel, and $\gamma = -1$ means that they flow in opposite directions.

The specific capacitance values are calculated by formulas (43) to (45). According to the subdivision of the program into the formulae (A I-1), (A I-2) and (A I-3) the output is organized in such a way ($d \neq r$) that for R, L and C three values are listed. The values are R_{21}, R_{22}, R_{20}, L_{21}, L_{22}, L_{20} and C_{21}, C_{22}, C_{20}. The index 21 corresponds to the central conductor, 22 to the return conductor and 20 to the total system.

Some results for the ASDEX UG "normal antenna" are shown in the following. The data are given in Section IV,4; the frequency is 80 MHz and the peak plasma density is $2 \cdot 10^{14}$ cm^{-3}. The distance d = 6 between the central conductor and vessel is kept constant.

For $\gamma = -1$ one can imagine that with decreasing r, R_{20} and L_{20} decreases because the flux between the two conductors decreases also.

In general the situation is more complex for L_{20}; there are two processes with opposing influences. The first one is the mentioned decrease between the two conductors (or between central conductor and vessel); this would yield a decrease of the magnetic flux and L_{20} if the magnetic field density remains the same as the case when the return conductor is integrated into the vessel. But on the other hand, with the decrease of r, the return conductor moves away from the vessel where the boundary condition $E_y = 0$, and therefore the current in the return
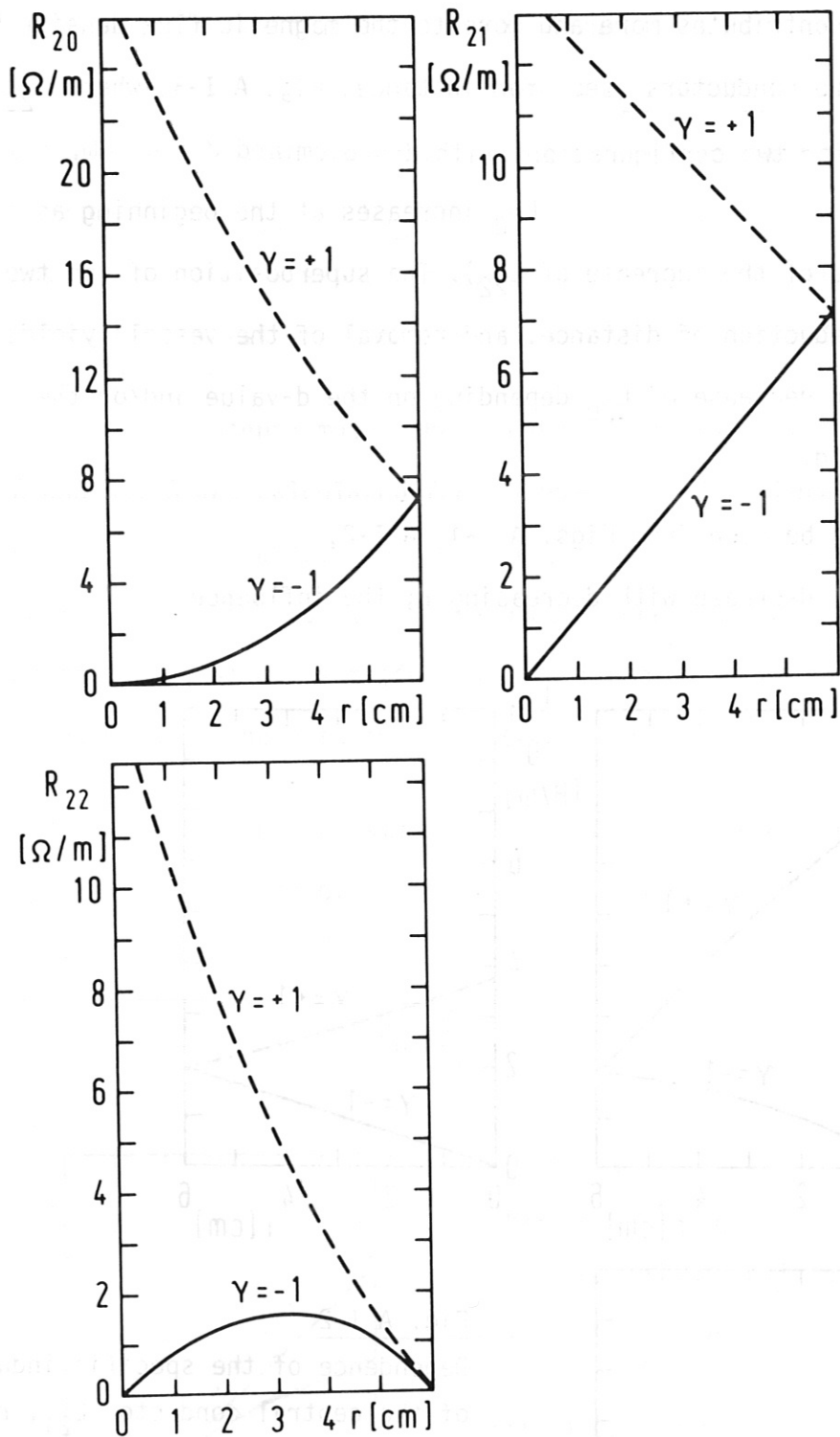
Fig. A I-1   Dependence of the specific resistivity of the central
conductor R_{21}, return conductor R_{22} and the total antenna R_{20}
as a function of the distance r between central conductor and
return conductor. With the exception of r the other data are
for the ASDEX UG "normal antenna" (see Section IV,4)
$\gamma = +1$ the currents are parallel (see remark on page 61)
$\gamma = -1$ the currents are antiparallel

conductor contributes more and more to the magnetic flux density bet-
ween the two conductors (see, for instance, Fig. A I-3, where L_{20}
is shown for two configurations with d = 6 cm and d = 60 cm.
. L_{20} increases at the beginning as a
consequence of the increase of L_{22}). The superposition of the two
effects (reduction of distance, and removal of the vessel) yields an
increase or decrease of L_{20} depending on the d-value and/or the
ratio of r/d.

As can be seen from Figs. A I-1, A I-2,
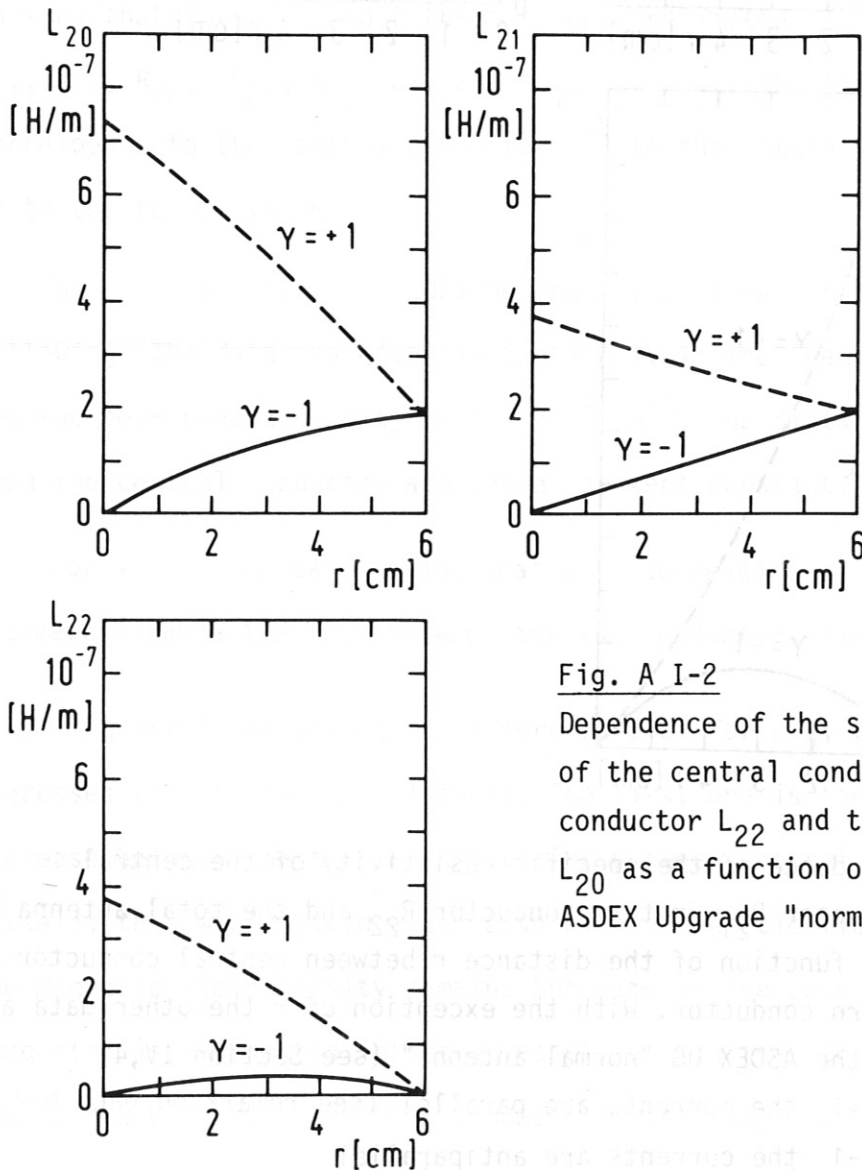R_{21} and L_{21} decrease with decreasing r; the influence

Fig. A I-2
Dependence of the specific inductance
of the central conductor L_{21}, return
conductor L_{22} and total antenna
L_{20} as a function of r for an
ASDEX Upgrade "normal antenna".

of the opposite current in the return conductor on the central conductor increases with decreasing distance. R_{22} and L_{22}, both small in comparison to R_{21} and L_{21} for $r > 2$ cm show a maximum at $r = d/2$. It is evident that R_{22} and L_{22} are zero when the return conductor is integrated into the vessel ($E_y = 0$, see Section II) and when the return conductor and central conductor are very near; they cancel each other.

For $\gamma = 1$ (antenna mode) the R and L values of figures A I-1, A I-2 and A I-3 are calculated for a current $I = I_s$, where I_s is the current in one conductor. The total current in the system consisting of the two conductors is $2I_s$; therefore, if one relates the R and L values to the total current (for calculation of Z_s, see eq.(54)) the R and L values have to be divided by four.

In Fig. A I-3 the transmission line mode ($\gamma = -1$) is compared with the specific inductance of an ideal transmission line for which L is given by

$$L = \mu_o \frac{r}{2w_z} \qquad \text{(A I-10)}$$
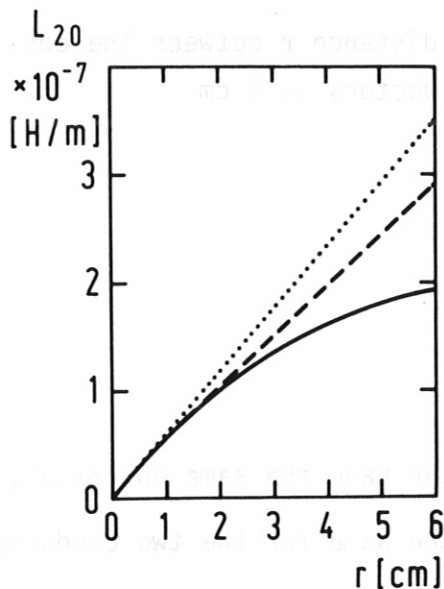
Fig. A I-3

Comparison of L_{20}

—— from Fig. A I-2 (d = 6 cm)

---- with removed vessel and plasma (d = a = 60 cm)

···· ideal transmission line

$2w_z$ is the width of the central conductor and for the return conductor. The distance between the two conductors is r. In Fig. (A I-3) the solid line represents the results where the vessel is 6 cm from the central conductor apart (curve from Fig. A I-2), the broken line gives L_{20} when the vessel and the plasma is removed about half a meter (d = a = 60 cm) and the dotted line shows the specific inductance calculated with formula (A I-10). The figure shows that with increasing r the deviations increase.

Finally we like to make a remark on the assumption used for the calculation model for the trombone antenna (see Section II).
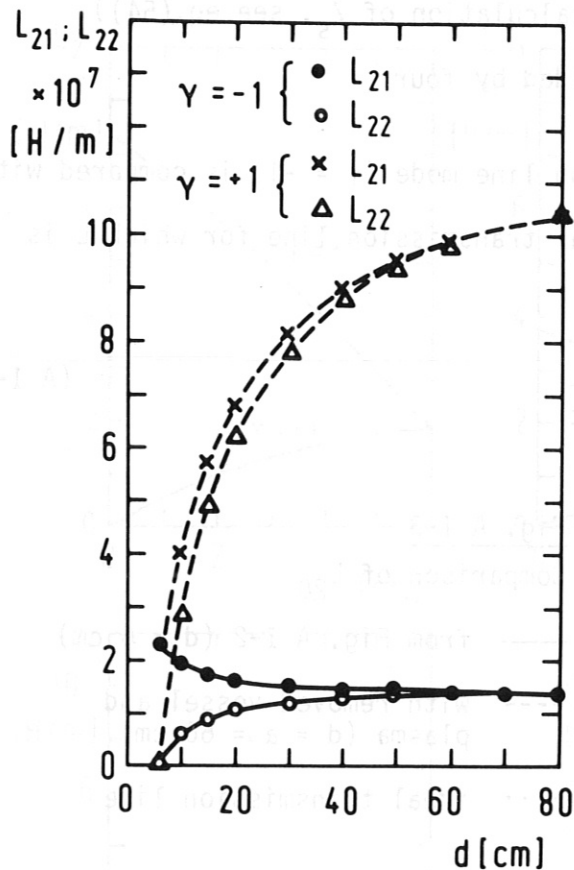

Fig. A I-4

The specific inductance for the central and "return conductor" versus the distance to the vessel. The plasma is removed (a = 60 cm) and the distance r between the conductors is 6 cm

One main assumption was that both conductor have the same potential, i.e. the induced electrical field E_y is the same for the two conductors; as can be seen from the boundary conditions (see description of the 2-D model) the vessel and the plasma disturbe the symmetry with respect to the two conductors.

To check the validity of the assumption of equal potential for the two conductors, L_{21} and L_{22} is calculated versus the distance d (distance between the central conductor and vessel). To eliminate the influence of the plasma on L, the distance a is set about half a meter.

From Fig. A I-4 one can see that for d < 20 cm there is a large difference especially for the transmission line mode.

In a forthcoming paper the influence of this assumption is discussed in more detail and a modified calculation model is described.

Appendix II

Hot Plasma Dispersion Relation

In this section the basic formulae used for the computer program developped are described and an example is given for an ASDEX plasma.

The underlying principle of the dielectric tensor can be found in Refs. /39, 40/.

A slab model is used, where the $\vec{E}$-vector lies in the x,z plane and $n_y = 0$. The RF electric fields are of the form

$$\vec{E} = \vec{E}_0 \exp i(k_\perp x + k_\parallel z - \omega t) \qquad \text{(A II-1)}$$

The generalized hot plasma dispersion relation is given by

$$
\begin{bmatrix}
(n_\perp^2 - n^2 + K_{xx}) & K_{xy} & n_\perp n_\parallel + K_{xz} \\
-K_{yx} & K_{xx} - n^2 + K_{yy} & K_{yz} \\
n_\parallel n_x + K_{zx} & -K_{zy} & K_{zz} - n^2 + n_\parallel^2
\end{bmatrix}
\begin{bmatrix}
E_x \\
E_y \\
E_z
\end{bmatrix} = 0
\qquad \text{(A II-2)}
$$

In (II-1) and (A II-2) n_x and n_z (or k_x, k_z) are replaced by $n_\perp$, $n_\parallel$ ($k_\perp$, $k_\parallel$).

The dispersion relation follows from (A II-2).

$$n^2 n_\perp^2 n_\parallel^2 (K_{xz}^+ + 2 K_{xz}^+) \cdot K_{zz}^{-1} - n_\perp^2 n_\parallel^4 K_{yz}^+ K_{zz}^{-1} + n^2 n_\parallel^2 + n^2 n_\perp^2 K_{xx} K_{zz}^{-1} + n_\perp^2 n_\parallel^2 K_{xx} K_{yz}^{2+} K_{zz}^{-1} -$$

$$- n_\perp^2 n_\parallel^2 (K_{xx} + K_{yy})(K_{xz}^{2+} + 2 K_{xz}^+) K_{zz}^{-1} + 2 n_\perp^2 n_\parallel^2 K_{xy} K_{yz}^+ (1 + K_{xz}^+) K_{zz}^{-1} - \qquad \text{(A II-3)}$$

$$- (n^2 + n_\parallel^2) K_{xx} - n_\parallel^2 K_{yy} - n_\perp^2 (K_{xx}^2 + K_{xy}^2 + K_{xx} K_{yy}) K_{zz}^{-1} + (K_{xx}^2 + K_{xy}^2) + K_{xx} K_{yy} = 0.$$

$$K_{xx} = 1 + \sum_{s} \frac{\omega_{ps}^2}{\omega k_{\shortparallel} v_s} \frac{e^{-\lambda_s}}{\lambda_s} \sum_{n=1}^{\infty} n^2 I_n (Z_n + Z_{-n})$$

$$K_{xy} = -i \sum_{s} \frac{\omega_{ps}^2}{\omega k_{\shortparallel} v_s} e^{-\lambda_s} \sum_{n=1}^{\infty} n(I_n - I_n') (Z_n - Z_{-n})$$

$$K_{yy} = 2\sum_{s} \frac{\omega_{ps}^2}{\omega k_{\shortparallel} v_s} \lambda_s e^{-\lambda_s} \{(I_0 - I_0')Z_0 + \sum_{n=1}^{\infty} (I_n - I_n')(Z_n + Z_{-n})\}$$

$$K_{xz}^+ = \sum_{s} \frac{\omega_{ps}^2 \, \omega}{2 \, \omega_{cs} \, k_{\shortparallel}^2 c^2} \frac{e^{-\lambda_s}}{\lambda_s} \sum_{n=1}^{\infty} n \, I_n (Z_n' - Z_{-n}') \qquad\qquad (A\ II\text{-}4)$$

$$K_{yz}^+ = -i \sum_{s} \frac{\omega_{ps}^2 \, \omega}{2\omega_{cs} k_{\shortparallel}^2 c^2} e^{-\lambda_s} \{(I_0' - I_0) Z_0' + \sum_{n=1}^{\infty} (I_n' - I_n)(Z_n' + Z_{-n}')\}$$

$$K_{zz} = 1 - \sum_{s} \frac{\omega_{ps}^2}{k^2 v_{\shortparallel s}^2} e^{-\lambda_s} \{I_0 Z_0' + \sum_{n=1}^{\infty} I_n [\frac{\omega + n \, \omega_{cs}}{\omega} Z_n' + \frac{(\omega - n \, \omega_{cs})}{\omega} Z_{-n}']\}$$

The elements with a + are normalized with respect to $n_{\shortparallel} n_{\perp}$ (for example $K_{xz}^+ = K_{xz}/n_{\perp} n_{\shortparallel}$) ρ is the gyroradius, Z_n is the plasma dispersion function of the argument $\xi_s = (\omega + n\omega_{cs})/k_{\shortparallel} v_s$, I_n is the modified Bessel function of the order n and of the argument $z = \lambda_s = k_{\perp}^2 \rho_s/2$ and the prime indicates differentiation with respect to the arguments of the plasma dispersion function or modified Bessel function. The symbol s describes the particle species.

The cyclotron-frequencies ω_c and plasma frequencies ω_p for ions and electrons are calculated with the following formulae:

Ions: $\qquad \omega_{cs} = - 0.9579 \cdot 10^8 \, Z_s \, B/A_s$

Electrons: $\omega_{ce} = 1.7588 \cdot 10^{11} \, B$ $\qquad\qquad$ (A II-5)

A_s : mass number (m_i/m_p)
Z_s : charge number
B : magnetic induction in T

Ions $\quad \omega_{ps} = 1.3165 \cdot Z_s \sqrt{n_s/A_s}$

Electrons: $\omega_{pe} = 5.6394 \cdot 10^1 \sqrt{n}$ $\qquad$ (A II-6)

n_s: density in m^{-3}

The thermal velocities v_{th} and the arguments λ_s for the Bessel function and the arguments ξ_s for the Plasma Dispersion Function are calculated with the following formulae:

Thermal velocities

Ions $\qquad v_s = 1.3848 \cdot 10^4 \sqrt{T_s/A_s}$

Electrons $\quad v = 5.9337 \cdot 10^5 \sqrt{T}$ $\qquad$ (A II-7)

T: temperature in eV; v, v_s in m/sec

Arguments for Plasma Dispersion Function

Ions $\quad \rho_{ns} = \dfrac{\omega - n\ 0.9579 \cdot 10^8\ Z_s\ B/A_s}{1.3848 \cdot 10^{11}\ \sqrt{T_s/A_s} \cdot k_{\parallel}}$

Electrons $\quad \rho = \dfrac{\omega + n\ 1.7588 \cdot 10^{11}\ B}{5.9337 \cdot 10^5\ k_{\parallel} \sqrt{T}}$ $\qquad$ (A II-8)

Arguments for the Bessel function

Ions $\quad \lambda_s = 1.1627 \cdot 10^{-25}\ n_{\perp}^2\ \omega^2\ A_s T_s/B^2\ Z_s^2$

Electrons $\quad \lambda = 6.3322 \cdot 10^{-29}\ n_{\perp}^2\ \omega^2\ T/B^2$ $\qquad$ (A II-9)

The infinite summations of (A II-4) are trunctated in the program for some n, such that the inequalities

$$I_n(\lambda)/I_o(\lambda) < 10^{-5}$$

and (A II-10)

$$\left| e^{-\lambda}\{I_o(\lambda) + 2 \sum_1^n I_n(\lambda)\} - 1 \right| < 10^{-5}$$

The second of these inequalities /41/ constitutes an independent check on the accuracy of $I_n(\lambda)$.

In the following the input of the computer program is described. Table A II-1 shows the data for an ASDEX plasma. The symbols are:

R_o: major radius in m

A: minor radius in m

BO: Magnetic induction value at the plasma centre (R = 0) in Tesla

OMEGA: $2\pi \cdot f$ (f $\equiv$ frequency)

K-Parallel: $k_\parallel$ in m^{-1}

NO: number of zeros

AO: initial value of R, where the program starts (AO = 0; plasma centre)

DR: increment of the R

NR: number of steps

TO: temperature in the plasma centre

XNO: density in the plasma centre.

If any of the Z, A, XNO values is zero for the ions (I = 2-10) the corresponding specimen do not contribute to the dispersion relation. The program is foreseen for ten species. Species I = 1 is always the electrons; the number of Z and A for the first line don't have influence.

```
TEST :  K-PAR = 1.46000 (ASDEX SECOND-HARMONIC)

RO (m)           :  1.4600
A  (m)           :  0.4000
BO (t)           :  2.2900
OMEGA            :  4.398229E+08
K-PARALLEL       :  1.466100E+00

NO (Nullstellen) :     2
AO               :  0.0200
DR               : -0.00200
NR               :    50
```

```
Teilchencharakteristik :   I      Z         A      TO(eV)  XNO(/m**3)
                           1   1.00000   1.00000   1500.   4.400E+19
                           2   1.00000   1.00000   2500.   4.400E+19
                           3   1.00000   2.00000      0.   0.000E+00
                           4   1.00000   1.00000   1000.   0.000E+00
                           5   1.00000   1.00000   1000.   0.000E+00
                           6   1.00000   1.00000   1000.   0.000E+00
                           7   8.00000  16.00000   1000.   0.000E+00
                           8   1.00000   1.00000   1000.   0.000E+00
                           9   1.00000   1.00000   1000.   0.000E+00
                          10   1.00000   1.00000   1000.   0.000E+00

       Davon 2 Teilchenarten ausgewählt :    1    2
```

Table A II-1: Input Data for Dispersion Program

Profiles for the magnetic induction, tempeatures and densities are used in the program; they can be changed by altering the relevant lines of the subprogram DISPERC. The magnetic induction follows from

$$B(R) = B_0/(1 + R/R_0) \tag{A II-11}$$

The temperature and density profiles (HTE and HXN) used for an ASDEX plasma are

$$HTE = 0.969 - 0.172 (R/A)^2 - 0.7884 (R/A)^4 \tag{A II-12}$$
$$HXN = 1.024 - 0.581 (R/A)^2 - 0.313 (R/A)^4 \tag{A II-13}$$

The profiles were calculated with the fit program AUSGLFP, using

measured ASDEX plasma profiles /42/; the calculated ones are shown

in Fig. A II-1.

The dispersion curves ($n_\parallel$ = 1) for an ASDEX plasma with the data collected

in Table A II-1 is shown in Fig. (A II-2) and Fig. (A II-3); the curves

(real- and imaginary part) of Fig. (A II.2) correspond to the fast

wave and that of Fig. (A II-3) to the Bernstein wave. In Fig. (A II-2)

the curve following from the cold plasma dispersion (rel. 7) is also

plotted, showing that at the outer part of the plasma there is no

noticeable difference between the cold and hot plasma dispersion.
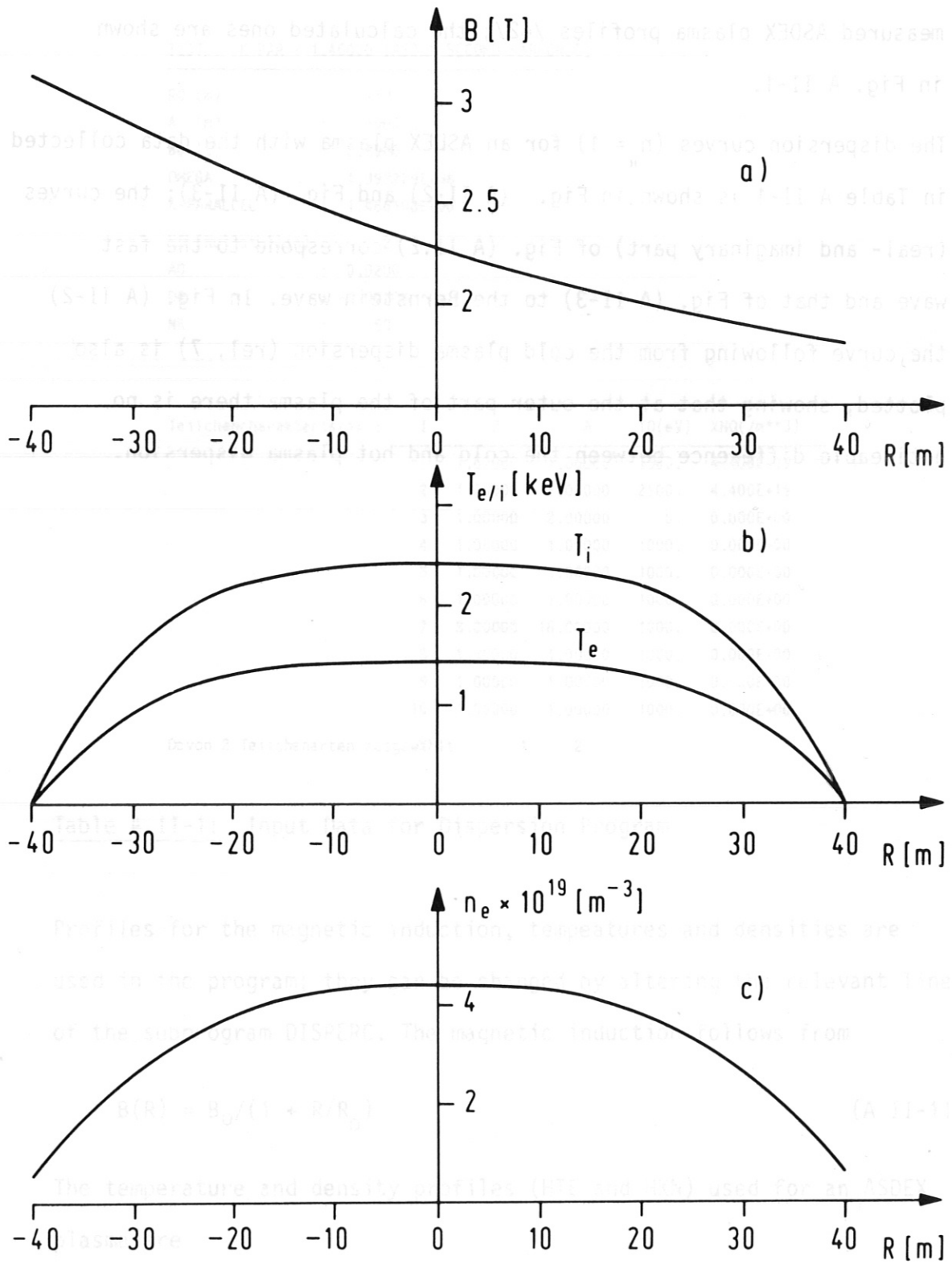
Fig. A II-1   Magnetic field (a), electron and ion temperature (b)
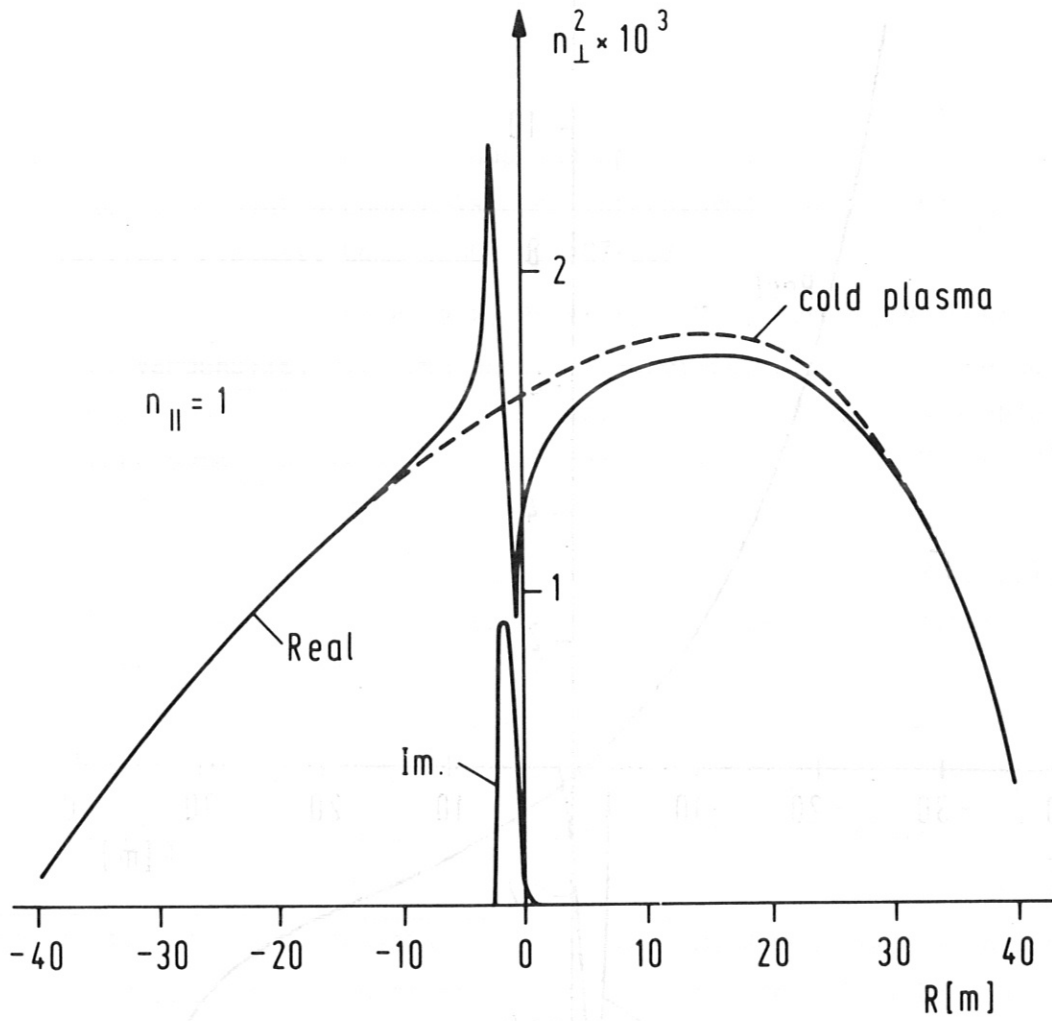and electron density profiles for an ASDEX plasma

Fig. A II-2 Local fast magnetosonic dispersion relation for an ASDEX (see Table A II-1) calculated with the "full hot dispersion relation" (solid lines) and with the "cold dispersion relation" (lined)
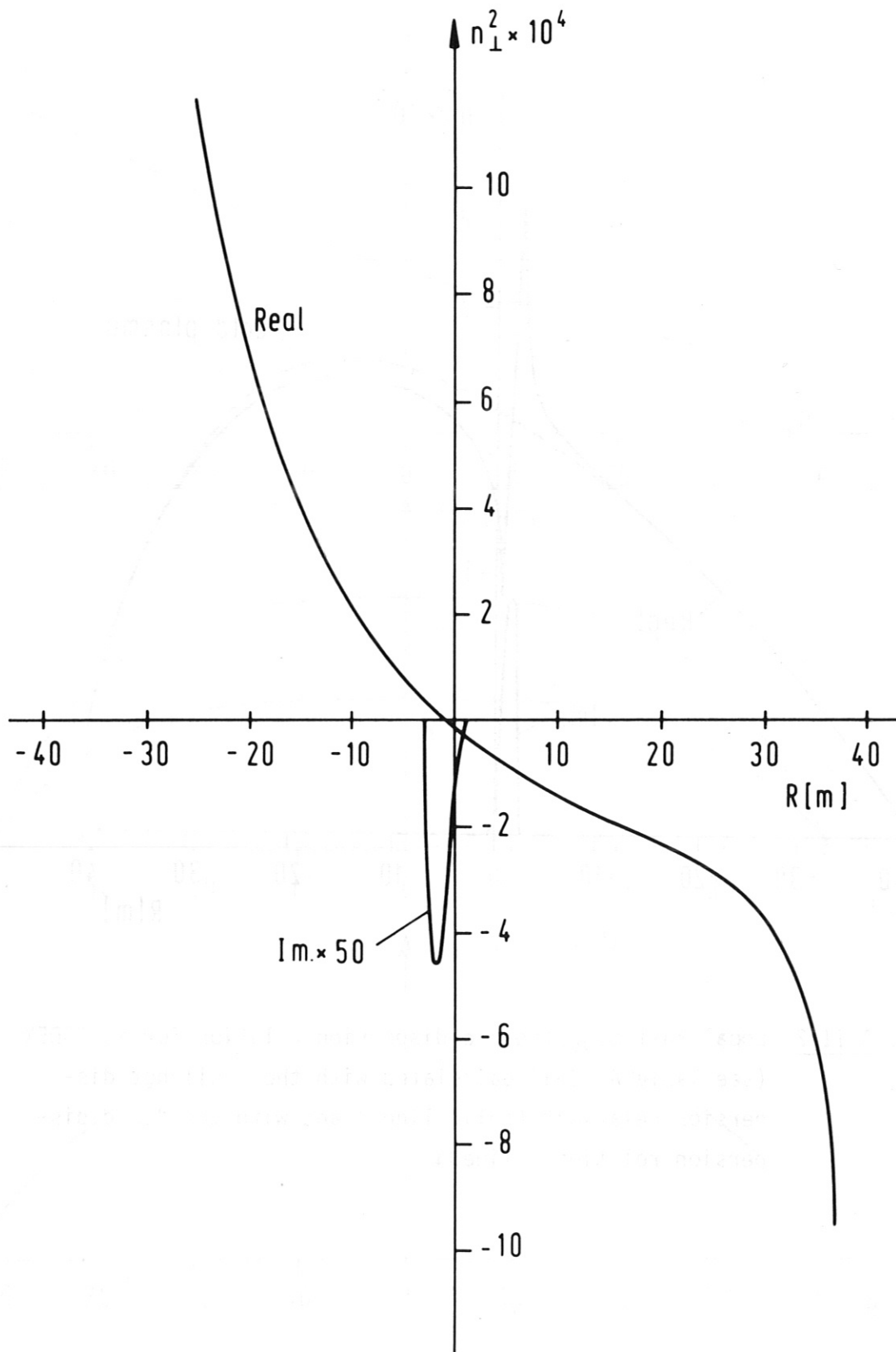
Fig. A II-3   Dispersion of the Ion-Bernstein wave for an ASDEX plasma

References

/1/ J. Adam: "Chauffage Cyclotronique Impedance d'Antenne en
     Presênce d'un Mechanisme de forte Absorption",
     Fontenay-aux-Roses, Report EUR-CEA-FC-1004, Mai 1979

/2/ R.R. Weynants, A.M. Messiaên, C. Leblud, P.E. Vandenplas:
     "ICRH antenna design and coupling optimization studies",
     Proc. 2nd Joint Grenoble-Varenna Intern.Symp. on Heating in
     Toroidal Plasmas, Como 1980, pp 487-507

/3/ A.M. Messiaen, R. Koch, V.P. Bhatnagar, M.P. Evrard, M. Luwel,
     P.E. Vandenplas, R.R. Weynants: "Theoretical aspects of the coupling
     properties of ICRH antennae", Proc. 3rd Joint Varenna-Grenoble
     Intern.Symp. on Heating in Toroidal Plasmas, Greoble, March 1982,
     pp 243-257

/4/ M.P. Evrard, V.P. Bhatnagar, D.W. Foulconer, R. Koch, M. Luwel,
     A.M. Messiaen, D.I.C. Pearson, P.E. Vandenplas, R.R. Weynants:
     "Theoretical Study of the JET Antenna Loading at the Ion Cyclotron
     Frequency", LPP-ERM/KMS Report No. 79, June 1982

/5/ V.P. Bhatnagar, R. Koch, A.M. Messiaen, R.R. Weynants: "A 3-D
     Analysis of the Coupling Characteristics of Ion Cyclotron
     Resonance Heating Antennae", Nucl. Fus., Vol. 22/2 (1982), pp 280-288

/6/ J. Jacquinot, K. Theilhaber, G. Lister, M. Brambilla: "Theory of
     a 3-D ICRF Antenna with Feeders and Finite Electrical Length:
     Coupling and Field Patterns in Large Inhomogeneous Plasmas",
     Proc. 3rd Joint Varenna-Grenoble Intern.Symp. on Heating in
     Toroidal Plasmas, Genoble, March 1982, pp. 375-381

/7/ K. Theilhaber, J. Jacquinot: "Variational Theory of ICRH Antenna",
     Report EUR-CEA-FC 1166, Nov. 1982

/8/ S. Puri: "Self-consistent, analytic, periodic-loop-antenna
     theory", Max-Planck-Institut für Plasmaphysik, Garching,
     Report IPP 4/214, November 1983

/9/ J. Hosea et al.: "High Power ICRF Heating on PLT and Extra-
     polation to Future Devices", Proc. 3rd Joint Varenna-Grenoble Intern.
     Symp. on Heating in Toroidal Plasmas", Grenoble, March 1982,
     pp 213-224

/10/ Equipe TFR: "ICRF Heating and Antenna Coupling Studies in TFR", Ibid, pp 225-242

/11/ JFT-2 Group: "ICRF Heating Experiment in JFT-2", Ibid, pp 259-273

/12/ D.W. Faulconer: "Adverse Magnetic Shielding and High Ohmic Loss Introduced by Antenna Shields Employed in RF-Heating", Ibid, pp 347-356

/13/ M.P. Evrad, R.R. Weynants: "ICRH Antenna Coupling to Slow Waves due to the Poloidal Field", Ibid, pp 339-346

/14/ V.P. Bhatnagar, D.W. Faulconer, R. Koch, D.I.C. Pearson: "Analysis of the Effect of Bump Limiters on the Coupling Properties of an ICRH Antenna", Ibid, pp 325-332

/15/ A. Messiaen, R. Weynants: "Design of ICRH Launching Structures: Antenna and Waveguide", Ibid, pp 1107-1116

/16/ A. Ram, A. Bers: "Antenna-Plasma Coupling Theory for ICRF Heating of Large Tokamaks", Ibid, pp 395-400

/17/ S. Puri: "Conducting Loop Antenna Theory", Ibid, pp 191-202

/18/ S. Puri: "Plasma Surface Impedance for Coupling to the Ion-Cyclotron and Ion-Bernstein Wave", Phys.Fluids, 26/1 (1983) pp 164-168

/19/ W.F. Baity, T.L. Owens: "Study of Power Coupling Through an Electrostatic Shield on a Loop Antenna for ICRF Heating of EBT-S", IEEE Transactions on Plasma Science, PS-11/1 (1983) pp 19-23

/20/ D.T. Blackfield, B.D. Blackwell: "A Numerical Investigation of ICRF Antenna Designs and Heating Schemes for Alcator-C", MIT, Report PFC/CP-83-4, Febr. 1983

/21/ G. Lisitano: "Radiofrequency Wave-Retarding Structures for Fusion Devices", Max-Planck-Institut für Plasmaphysik, Garching, Bericht IPP III/87, April 1983

/22/ F. Braun, M. Söll, J.M. Noterdaeme: "Comparison of Experimental and Calculated ICRH Antenna Parameters", Proc. 10th Symp. on Fusion Engineering, Philadelphia (1983), pp 539-543

/23/ Y. Lapierre: "Magnetosonic wave propagation in the mode conversion regime", J. Plasma Physics, 29/2 (1983) pp 223-241

/24/ M. Söll: "ICRH Antenna Design Calculation for ASDEX and W VII-A",
     Proc. 3th Joint Varenna-Grenoble Intern.Symp. on Heating in
     Toroidal Plasmas, Grenoble, March 1982, pp 415-422

/25/ F. Wesner, F. Braun, R. Fritsch, F. Hofmeister, E. v.Mark, M. Söll,
     H. Wedler: "ICRH for ASDEX and W VII", Ibid, pp 429-435

/26/ F. Braun, R. Fritsch, F. Hofmeister, E. v.Mark, S. Puri, M. Söll,
     F. Wesner, H. Wedler: "Design of a 3 MW ICRH System for ASDEX
     and W VII", Proc. 12th Symp. on Fusion Technology, Jülich, Sept. 1982,
     Vol. II, pp 1393-1398

/27/ V.P. Bhatnagar, L. Bral, R. Koch, A.M. Messiaen, D.I.C. Pearson,
     P.E. Vandenplas, G. van Oost, R.R. Weynants, N. Maene, F. Moons,
     W. Kohlhaas, C. Stickelmann: "The high power long pulse ion cyclotron
     resonance heating system for TEXTOR", Ibid., Vol. II, pp 1275-1282

/28/ P.H. Rebut: "JET Joint Undertaking: March 1982", Proc. 3th Joint
     Varenna-Grenoble Intern. Symp. on Heating in Toroidal Plasmas,
     Grenoble, March 1982, Vol. III, pp 989-998

/29/ Y. Shimomura, S. Matsuda, T. Nagashima: "NBI and RF Heating
     of JT-60", Ibid, Vol. III, pp 1007-1014

/30/ R. Aymar: "Supplementary Heating in Tore Supra", Ibid, Vol. III,
     pp 953-959

/31/ ASDEX Upgrade Project Team: "ASDEX Upgrade Project Proposal;
     Phase II", Max-Planck-Institut für Plasmaphysik, Garching,
     Report IPP 1/217, Mai 1983

/32/ R.R. Weynants: "The Heating of INTOR by Ion Cyclotron Frequency
     Heaging", LPP-ERM/KMS, Report No. 80, Oct. 1982

/33/ F.W. Perkins, R.F. Kluge: "A Resonant Cavity ICRF Coupler for
     Large Tokamaks, Princeton University, Report PPPL-2000, April 1983.

/34/ S. Puri: "Lower-hybrid wave absorption in the presence of
     simultaneous density and magnetic field gradients",
     Phys. Fluids 22 (1979) 1716

/35/ J.E. Storer: "Solution of thin wire antenna problems by
     variational methods". Thesis, Cambridge, June 1951

/36/ A.M. Messiaen, R. Meynart, R.R. Weynants: "Etude d'un modele bidimensional pour le calcul de l'impedance d'une antenne ICRH. Application an cas de la machine Textor", Lab.Rep. 76 (1981)

/37/ L. Bral, G. van Oost: "Experimental investigations of the shielding of the heating field by the electrostatic shield of a stripline ICRF-antenna", IEEE Tr. on Magnetics, PS-11/4, 1983, pp 251-254

/38/ R.E. Collins: "Foundations for Microwave Engineering", McGraw-Hill, 1966, International Student Edition, p. 91

/39/ T.H. Stix: "The Theory of Plasma Waves", New York, McGraw-Hill, 1962

/40/ J.E. Scharer, J.B. Beyer, D.T. Blackfield, T.K. Mau: "Fast Magnetosonic-Wave Heating in the Concentual NUWMAK Tokamak Reactor", Nucl.Fus. 19 (1979) 1171

/41/ M. Abramovitz, I.A. Stegun: "Handbook of Mathematical Functions", National Bureau of Standards, 1964, § 9.6.37

/42/ ASDEX-Team: private communication

/43/ W.L. Stutzmann, G.A. Thiele: "Antenna Theory and Design, John Wiley & Sons, 1981

/44/ S. Ramo, J. Whinnery, T. Vandizer: "Fields and Waves in Communication Electronics", John Wiley & Sons, 1965

/45/ M. Söll, F. Wesner: "ICRH antenna design for the ASDEX and ASDEX UPGRADE tokamaks and for the W VII stellarators", Proc. 10th Symposium on Fusion Engineering, Philadelphia 1983, pp. 600-604

/46/ J.-M. Noterdaeme, F. Braun, M. Söll: "Innovative designs for long pulse ICRH antenna". 4th Int.Conf. on Heating in Toroidal Plasmas, Rome 1984

/47/ P.H. Morse, H. Freshbach: "Methods of Theoretical Physics", McGraw-Hill, 1953